Cell Reports

Article

Neural circuits and activity dynamics underlying sex-specific effects of chronic social isolation stress

Graphical abstract

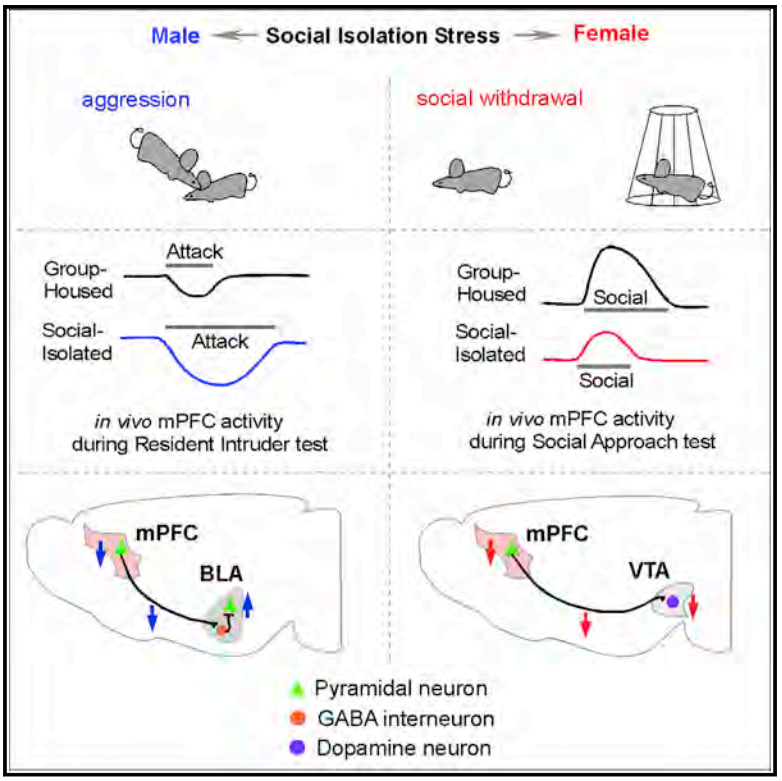

Authors

Tao Tan, Wei Wang, Tiaotiao Liu, Ping Zhong, Megan Conrow-Graham, Xin Tian, Zhen Yan

Correspondence

zhenyan@buffalo.edu

In brief

Tan et al. use *in vivo* multichannel recordings of free-moving mice, *ex vivo* recordings of brain slices, and chemogenetics to reveal the circuit and physiological mechanisms underlying the sex-specific effects of chronic adolescent social isolation stress: heightened aggression in stressed males and social withdrawal in stressed females.

Highlights

- Stressed males exhibit heightened aggression and dampened PFC activity during attack
- Stressed females exhibit social withdrawal and blunted PFC activation by social stimuli
- DREADD normalization of PFC and BLA activity in stressed males mitigates aggression
- DREADD normalization of PFC and VTA activity in stressed females rescues social deficits

Tan et al., 2021, Cell Reports *34*, 108874
March 23, 2021
https://doi.org/10.1016/j.celrep.2021.108874

CellPress

Cell Reports

CellPress
OPEN ACCESS

Article

Neural circuits and activity dynamics underlying sex-specific effects of chronic social isolation stress

Tao Tan,[1] Wei Wang,[1] Tiaotiao Liu,[1,2] Ping Zhong,[1] Megan Conrow-Graham,[1] Xin Tian,[2] and Zhen Yan[1,3,*]

[1]Department of Physiology and Biophysics, Jacobs School of Medicine and Biomedical Sciences, State University of New York at Buffalo, Buffalo, NY 14203, USA

[2]School of Biomedical Engineering and Technology, Tianjin Medical University, Tianjin 300070, China

[3]Lead contact

*Correspondence: zhenyan@buffalo.edu

https://doi.org/10.1016/j.celrep.2021.108874

SUMMARY

Exposure to prolonged stress in critical developmental periods induces heightened vulnerability to psychiatric disorders, which may have sex-specific consequences. Here we investigate the neuronal circuits mediating behavioral changes in mice after chronic adolescent social isolation stress. Escalated aggression is exhibited in stressed males, while social withdrawal is shown in stressed females. *In vivo* multichannel recordings of free-moving animals indicate that pyramidal neurons in prefrontal cortex (PFC) from stressed males exhibit the significantly decreased spike activity during aggressive attacks, while PFC pyramidal neurons from stressed females show a blunted increase of discharge rates during sociability tests. Chemogenetic and electrophysiological evidence shows that PFC hypofunctioning and BLA principal neuron hyperactivity contribute to the elevated aggression in stressed males, while PFC hypofunctioning and VTA dopamine neuron hypoactivity contribute to the diminished sociability in stressed females. These results establish a framework for understanding the circuit and physiological mechanisms underlying sex-specific divergent effects of stress.

INTRODUCTION

Stress hormones elicit profound and complex effects throughout the lifespan (de Kloet et al., 2005; Lupien et al., 2009; McEwen and Morrison, 2013; Popoli et al., 2011). The adolescent brain is particularly sensitive to stressors because of the dramatic hormonal and neurodevelopmental changes around puberty (Lupien et al., 2009; McEwen and Morrison, 2013; Paus et al., 2008). In humans, early adversity, such as emotional neglect, social exclusion, and peripubertal stress, contributes significantly to the abnormal aggressive and antisocial behaviors, as well as anxiety and depressive disorders (Anderson et al., 1999; Davidson et al., 2000; Fries et al., 2008; Heim and Nemeroff, 2001; Marín, 2016). Animal models of early life stress, such as repeated maternal separation, post-weaning social isolation, and unpredictable stress during adolescence, also capitulate many behavioral symptoms similar to those in humans (Burke et al., 2017; Haller et al., 2014; Liston et al., 2009; Márquez et al., 2013; Niwa et al., 2013; Yuen et al., 2012). Stress hormones are dramatically disturbed by chronic social isolation (Malkesman et al., 2006; Mucignat-Caretta et al., 2014; Sayegh et al., 1990).

One important but understudied question is the sexually dimorphic effects of early life stress. Most animal studies on adolescent social isolation stress have focused on males, which exhibit elevated anxiety, susceptibility to addiction-related behaviors, and aggression (Tóth et al., 2008; Zelikowsky et al., 2018). Relatively little is known about how females respond to isolation stress (Walker et al., 2019). In humans, the prevalence of aggression and violence is significantly higher in men, while the prevalence of depression is significantly higher in women. Recent findings suggest that stress exerts diverse behavioral, emotional, and transcriptional impacts in males and females (Bale and Epperson, 2015; Farrell et al., 2013; Hodes et al., 2015; Labonté et al., 2017; Peña et al., 2019; Wei et al., 2014; Wellman et al., 2018).

The human brain has sex differences in the structural connectome (Ingalhalikar et al., 2014). To understand the physiological basis of the diverse effects of stress in both sexes, it is critical to determine the neuronal circuits controlling different consequences of stress. Brain imaging has revealed the altered activity in specific regions, such as the amygdala and the medial orbitofrontal cortex, in aggressive-impulsive human individuals (Coccaro et al., 2007, 2011; Raine et al., 1997), but the results are largely correlational rather than deterministic. Here we use *in vivo* recordings of neuronal spikes in behaving animals and chemogenetics to interrogate neural activity in three interconnected key target regions of stress involved in aggression, sociability, and mood disorders: prefrontal cortex (PFC), basolateral amygdala (BLA), and ventral tegmental area (VTA) (Davidson et al., 2000; Gold, 2015; McEwen and Morrison, 2013; McEwen et al., 2016; Popoli et al., 2011; Zhang and Li, 2018). PFC serves as the command center controlling higher level "executive"

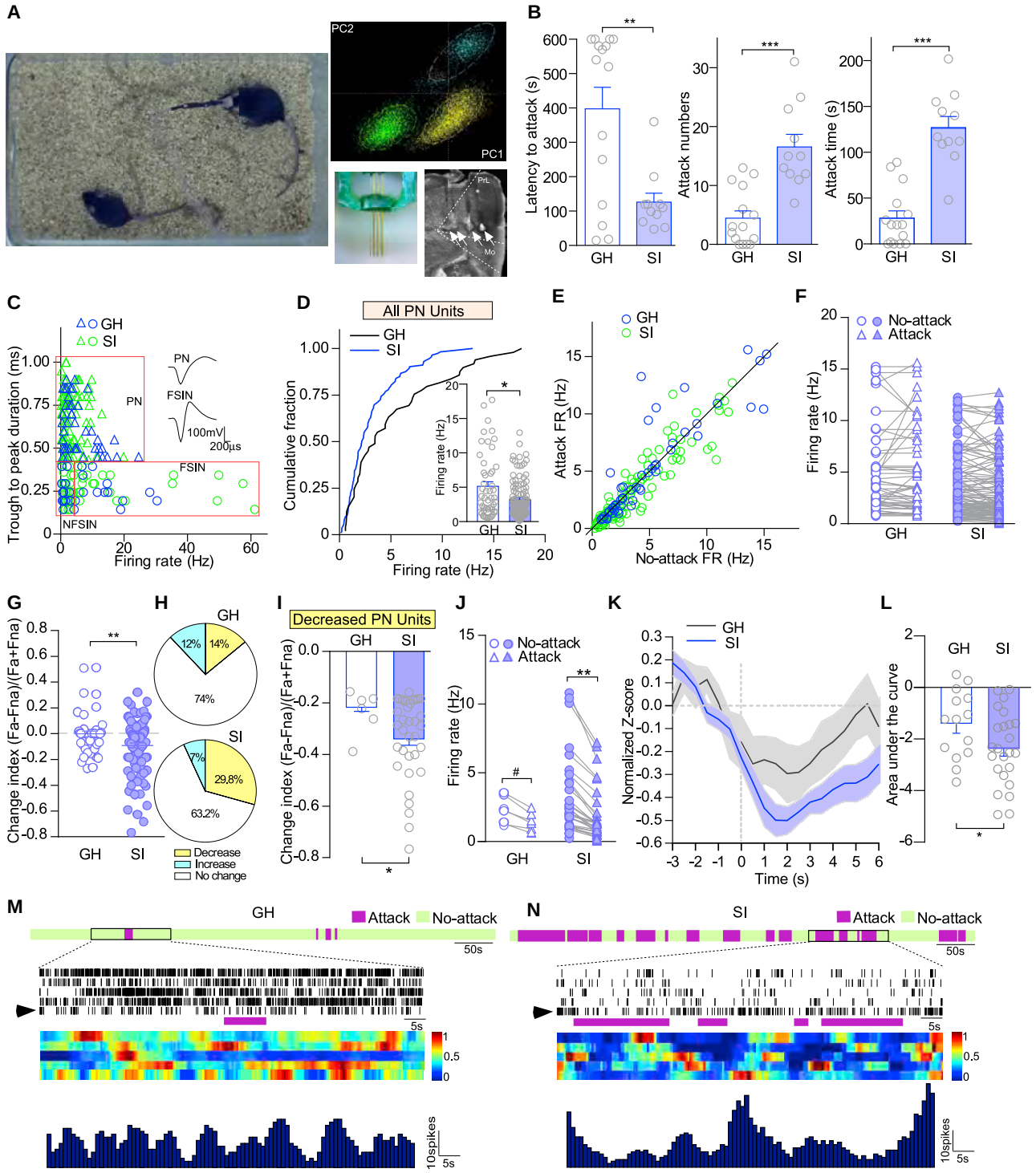

Figure 1. Male mice exposed to isolation stress have elevated aggression and dampened spike activity in PFC pyramidal neurons during attacks in the resident-intruder (RI) test

(A) *In vivo* multi-channel recording of a male mouse during the RI test (left), three well-isolated single units (yellow, green, and blue clusters) from the recording of medial PFC (mPFC) (top right), a 16-channel electrode for *in vivo* recordings (bottom right), and micrograph showing electrode implantation into mPFC (white arrows, bottom right).

(B) Bar graphs showing aggressive behaviors of group-housed (GH; n = 15) and single-housed socially isolated (SI; n = 11) male mice in the RI test (latency to attack: p = 0.01, Mann-Whitney [M-W] test; attack numbers: p < 0.001, t test; attack time: p < 0.001, t test).

(legend continued on next page)

functions, including working memory, decision making, social cognition, and emotional control (Davidson et al., 2000; Hiser and Koenigs, 2018; Ridderinkhof et al., 2004). We speculate that aggression or social withdrawal behavior arises as a consequence of faulty emotion regulation because of dysfunctional PFC and its connected neural circuitry. Results gained from this study will aid in understanding the physiological basis of sexually dimorphic effects of stress.

RESULTS

Chronic isolation stress induces aggression in males, correlating with the dampened activity in PFC pyramidal neurons during attacks

To examine the impact of stress in both sexes, we exposed young mice (3 weeks old) to chronic isolation stress (single-housed for 5 weeks) (Walker et al., 2019) and compared group-housed control (GH) and social isolation stressed (SI) mice of either sex (Figure S1A). We first measured the effects of SI on aggression, a behavioral change induced by various stressors (Márquez et al., 2013; Tóth et al., 2008; Wei et al., 2018; Zelikowsky et al., 2018). The resident-intruder (RI) test (Wei et al., 2018), a classic behavioral assay for reactive aggression, was used during *in vivo* multichannel recordings of neuronal spike activity (Figure 1A). Behavioral tests revealed that compared with GH male mice, SI male mice had a significantly shorter latency to the first attack, larger numbers of attacks, and longer duration of attack (Figure 1B), indicating escalated aggression level. However, no significant change in aggression was found in SI female mice (Figures S1B–S1D).

To find out what drives the aggressive behavior in SI males, we examined PFC neuronal activity using single-unit recordings of freely behaving animals, as PFC plays a key role in regulating stress-induced excessive aggressive behaviors (Nelson and Trainor, 2007; Takahashi et al., 2014). Sixteen-channel multi-electrode arrays (4 × 4) (Liu et al., 2014b, 2018) were used to target medial PFC (mPFC), including prelimbic (PrL) and infralimbic (IL), and electrode placement was confirmed histologically post hoc (Figure 1A). We recorded a total of 228 well-isolated units (73 from 7 GH male mice, 155 from 15 SI male mice), including 164 pyramidal neurons (PNs; 71.9%), 26 fast-spike narrow-spiking interneurons (FSINs), and 38 non-fast-spike narrow-spiking interneurons (NFSINs) (Xu et al., 2019) (Figure 1C).

We then compared the spike rates of mPFC PNs in GH and SI males during RI tests. The average firing frequency of recorded PN units at baseline (3 min before RI tests) was significantly lower in SI than GH mice (Figure 1D). In RI tests, the mean firing rate during attack epochs relative to no-attack epochs showed the mixed changes, with increase, decrease, and no alteration in different PN units (Figures 1E and 1F). Quantification of the attack-associated firing rate change index (CI) (Zhou et al., 2017) demonstrated a significant decrease in PN units from SI males compared with GH males (Figure 1G). As summarized in Figure 1H, SI males had more PN units with the decreased firing rate during the attack (GH, 14.0%; SI, 29.8%) and fewer PN units with the increased firing rate during the attack (GH, 12.0%; SI, 7.0%). Further examination of the decreased PN units revealed that this cell population in SI males had significantly more reduction in the firing rate (Figures 1I and 1J). These PN units from SI males also showed larger negative areas under the normalized activity (*Z* score) (Diehl et al., 2018) curves between onset (0 s) and 6 s after the attack (Figures 1K and 1L). Recordings of representative PN units from GH and SI males indicated that spike rates were largely unchanged during the short attacks in GH males (Figure 1M), while prominent reductions of spike rates were well correlated with the initiation and execution of prolonged aggressive attacks in SI males (Figure 1N). In contrast to these changes in PN units of SI males, no significant changes were observed in the recorded FSIN and NFSIN units (Figure S2). These data suggest that the elevated aggression in SI males is accompanied with the diminished activity of a population of PFC PNs.

Chronic isolation stress induces social withdrawal in females, correlating with the blunted activation of PFC pyramidal neurons by social stimuli

We next measured the effects of chronic isolation stress on sociability, another behavioral change often linked to various stressors (Farrell et al., 2016; Greenberg et al., 2015). The social

(C) Classification of recorded mPFC units from GH and SI males into wide-spiking putative pyramidal neurons (PNs; triangles), non-fast spike and narrow-spiking interneurons (NFSINs; circles at bottom left), and fast- and narrow-spiking interneurons (FSINs; circles at bottom right). Inset: representative spike waveforms of a PN and an FSIN.

(D) Distribution plots of the average firing frequency of all PN units at baseline (3 min before the RI test) in GH (n = 50 units, 7 mice) and SI (n = 114 units, 15 mice) males ($p = 0.01$, M-W test).

(E and F) Scatterplots of the firing rates of all PN units during attack against no-attack epochs in the RI test of GH and SI mice.

(G) Scatterplots of attack-associated firing rate change index (CI; [Fa − Fna]/[Fa + Fna]) of all PN units ($p = 0.002$, Kolmogorov-Smirnov [K-S] test). Fa, firing rate during attack; Fna, firing rate during no-attack.

(H) Pie graphs showing the proportions of PN units with an increase ($CI \geq 0.15$), decrease ($CI \leq -0.15$), or no change ($-0.15 < CI < 0.15$) of firing rate during attack relative to no-attack epochs in GH and SI males ($p = 0.08$, chi-square test).

(I) Bar graphs of CI in the subpopulation of decreased PN units from GH (n = 6 units) and SI (n = 34 units) males ($p = 0.05$, M-W test).

(J) Scatterplots of the firing rates of the subpopulation of decreased PN units during attack and no-attack epochs in the RI test of GH and SI males ($F_{[1, 38]} = 24.2$, $p < 0.001$, two-way repeated-measures ANOVA [rmANOVA]).

(K) Plots of normalized firing responses (*Z* score) of the subpopulation of decreased PN units from GH and SI males.

(L) Bar graphs of the area under the normalized *Z* score curves (between attack onset [0 s] and 6 s after attack) of the subpopulation of decreased PN units from GH and SI males ($p = 0.04$, t test).

(M and N) Representative behavioral and *in vivo* recording data from a GH (M) and an SI (N) male during the RI test. Top: raster plots of behaviors showing attack (purple) and no-attack (green) epochs; bottom: raster plots, heatmaps, and histogram of spikes of PN units within the time windows containing attacks (10–15 s before and after a single or series of attack epochs). Purple lines indicate the attack epochs. Arrowheads point to the units used for the generation of histograms. #$p < 0.1$, *$p < 0.05$, **$p < 0.01$, and ***$p < 0.001$. All data were presented as means ± SEM. See also Figures S1 and S2.

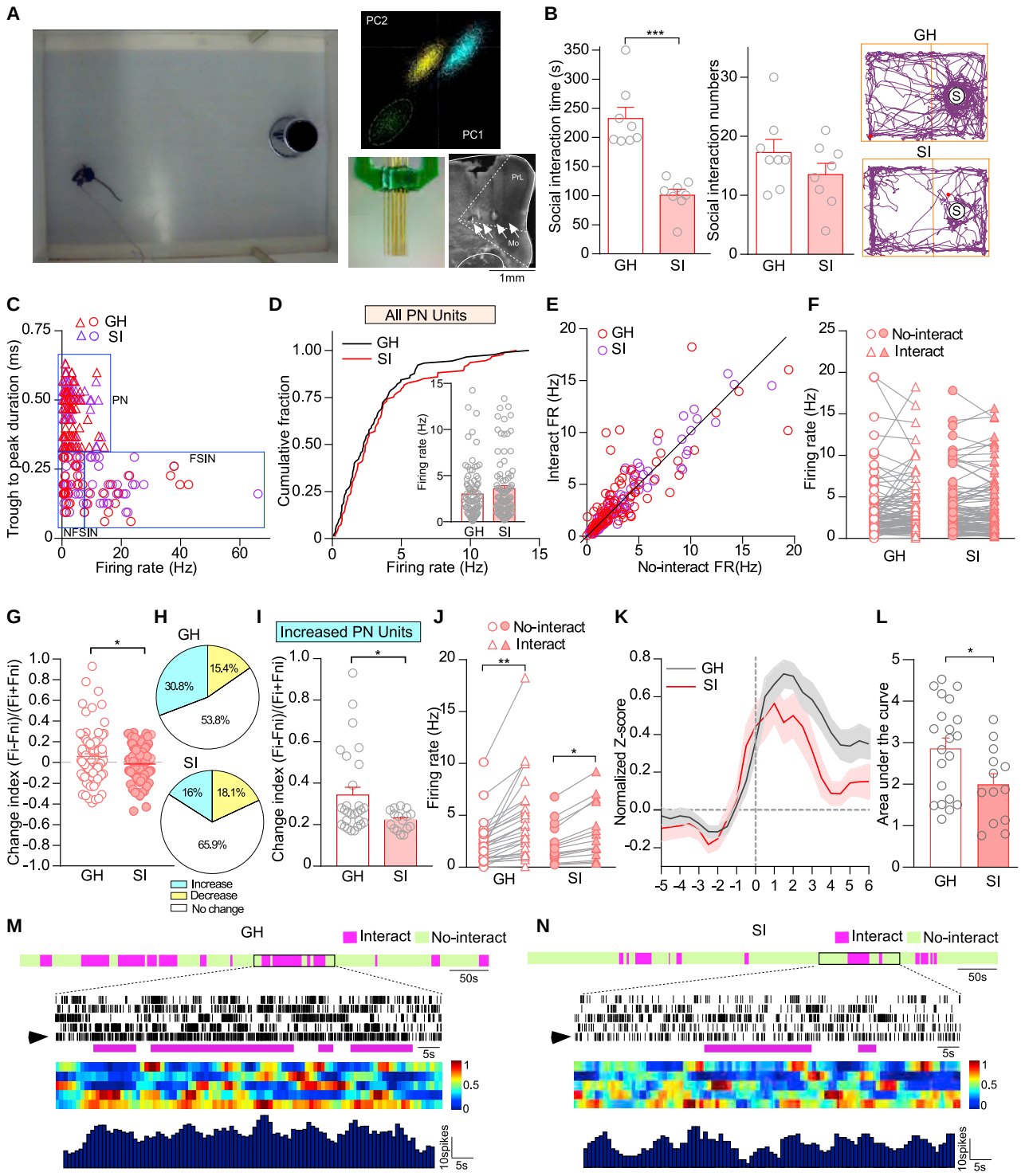

Figure 2. Female mice exposed to isolation stress exhibit social deficits and blunted activation of PFC pyramidal neurons by social stimuli in the social approach (SA) test

(A) *In vivo* multi-channel recording of a female mouse during the SA test (left), three well-isolated single units (yellow, green, and blue clusters) from the recording of mPFC (top right), a 16-channel electrode for *in vivo* recordings (bottom right), and micrograph showing electrode implantation into mPFC (white arrows, bottom right).

(B) Bar graphs showing social interaction behaviors of GH (n = 8) and SI (n = 8) females in the SA test (interaction time: $p < 0.001$, t test). Inset: representative movement traces of a GH and an SI female mice in a SA test. S, social stimulus.

(legend continued on next page)

approach (SA) test (Tan et al., 2019) was performed during *in vivo* multichannel recordings of neuronal spike activity (Figure 2A). Compared with GH females, SI females exhibited significantly shorter interaction time with social stimuli (Figure 2B), suggesting the presence of social deficits. In contrast, no obvious sociability change was noted in SI male mice (Figures S1E–S1G).

To find out what drives social withdrawal in SI female, we carried out single-unit recordings of PFC neuronal activity on freely behaving animals, as PFC is the key region highly implicated in social engagement (Jennings et al., 2019; Kim et al., 2015; Lee et al., 2016; Minami et al., 2017). A total of 276 well-isolated units (124 from 8 GH female mice, 152 from 12 SI female mice) was recorded, which was composed of 185 putative PNs (67.0%), 40 FSINs, and 51 NFSINs (Figure 2C).

We then compared the spike activity of mPFC PNs in GH and SI females during SA tests. The average firing frequency of recorded PN units at baseline (5 min before SA tests) showed no difference between GH and SI female mice (Figure 2D). In SA tests, the mean firing rate during social interaction epochs relative to no-interaction epochs showed the mixed changes, with increase, decrease, and no alteration in different PN units (Figures 2E and 2F). Quantification of the interaction-associated firing rate CI demonstrated a significant increase in PN units from GH females, but not SI females (Figure 2G). As summarized in Figure 2H, SI females had fewer PN units with the increased firing rate during interaction (GH, 30.8%; SI, 16.0%) and slightly more PN units with the decreased firing rate during interaction (GH, 15.4%; SI, 18.1%). Further examination of the increased PN units revealed that this cell population in SI females had significantly less enhancement of the firing rate than GH females (Figures 2I and 2J). These PN units from SI females also showed smaller areas under the normalized *Z* score curves between onset (0 s) and 6 s after the interaction (Figures 2K and 2L). Recordings of representative PN units from GH and SI females indicated that a prominent increase of spike rates were well correlated with the initiation and execution of continuous social engagement in GH females (Figure 2M), while spike rates were largely unchanged during the short interactions in SI females (Figure 2N). In contrast to the changes in PN units, no significant changes were found in recorded FSIN and NFSIN units from SI females (Figure S3). Together, these results suggest that social withdrawal in SI females is correlated with the blunted activation of a population of PFC PNs by social stimuli.

In stressed males, chemogenetic stimulation of PFC restores PFC pyramidal neuronal activity during intruder tests and mitigates aggressive behavior

Given the link between the elevated aggression and the diminished activity of PFC PNs in SI males, we next examined whether increasing PFC neuronal activity is capable of mitigating the aggressive behavior. The CaMKII promoter-driven, mCherry-tagged adeno-associated virus (AAV) expressing hM3D (Gq), a designer receptor exclusively activated by designer drugs (DREADD) (Roth, 2016), was injected into mPFC (Figure 3A) to activate PNs (Wang et al., 2018).

We first assessed *in vivo* spike activity of saline- or CNO-injected (3 mg/kg, intraperitoneal [i.p.]) GH and SI males (with hM3Dq in mPFC) while conducting the RI test. Among all the recorded PN units, CNO administration did not significantly alter the baseline firing (Figure 3B). However, a subpopulation of PN units from SI males showed the significantly elevated activity after CNO application, compared with saline treatment (Figure 3C), confirming the capability of hM3Dq to activate PFC PNs. In RI tests, CNO treatment of SI males normalized the discharge activity during attack epochs relative to no-attack epochs (Figures 3D–3H) and prevented the attack-associated reduction of firing rate (Figure 3F). Moreover, CNO treatment of SI males balanced the proportion profile, with fewer PN units showing the decreased firing rate during the attack (SI + saline, 35.4%; SI + CNO, 22.5%) and more PN units showing the increased firing rate during the attack (SI + saline, 7.7%; SI + CNO, 16.3%) (Figure 3G). Further examination of the decreased PN units revealed that CNO treatment attenuated the reduction of spike frequency of this cell population in SI males (Figure 3H). Correlating with the rescuing effect of CNO on *in vivo* neuronal activity, CNO treatment also significantly reduced aggression, as demonstrated by the lower numbers and shorter durations of attacks in RI tests (Figure 3I). However, in SI males with no-DREADD controls, CNO injection failed to reduce the heightened aggression (Figure 3I).

(C) Classification of recorded mPFC units from GH and SI females into PNs (triangles), NFSINs (circles at bottom left), and FSINs (circles at bottom right).
(D) Distribution plots of the average firing frequency of all PN units at baseline (5 min before the SA test) in GH (n = 91 units, 8 mice) and SI (n = 94 units, 12 mice) females.
(E and F) Scatterplots of the firing rates of all PN units during social interaction against no-interaction epoch in the SA test of GH and SI females.
(G) Scatterplots of social interaction-associated firing rate change index (CI; [Fi − Fni]/[Fi + Fni]) of all PN units ($p = 0.03$, M-W test). Fi, firing rate during social interaction; Fni, firing rate during no-interaction.
(H) Pie graphs showing the proportions of PN units with an increase, decrease, and no change of firing rate during social interaction epochs relative to no-interaction in GH and SI females ($p = 0.06$, chi-square test).
(I) Bar graphs of the CI in the subpopulation of increased PN units from GH (n = 28 units) and SI (n = 16 units) females ($p = 0.02$, M-W test).
(J) Scatterplots of the firing rates of the subpopulation of increased PN units during social interaction and no-interaction epochs in the SA test of GH and SI females ($F_{[1, 42]} = 3.6$, $p = 0.065$, two-way rmANOVA).
(K) Plots of normalized *Z* score of the subpopulation of increased PN units from GH and SI females.
(L) Bar graphs of the area under the normalized *Z* score curves (between social interaction onset [0 s] and 6 s after interaction) of the subpopulation of increased PN units from GH and SI females ($p = 0.04$, t test).
(M and N) Representative behavioral and *in vivo* recording data from a GH (M) and an SI (N) female during the SA test. Top: raster plots of behaviors showing social interaction (purple) and no-interaction (green) epochs; bottom: raster plots, heatmaps, and histogram of spikes of PN units within the time windows containing social interaction (10–15 s before and after a single or series of interaction epochs). Purple lines indicate the social interaction epochs. Arrowheads point to the units for the generation of histograms.
*$p < 0.05$, **$p < 0.01$, and ***$p < 0.001$. All data were presented as means ± SEM. See also Figures S1 and S3.

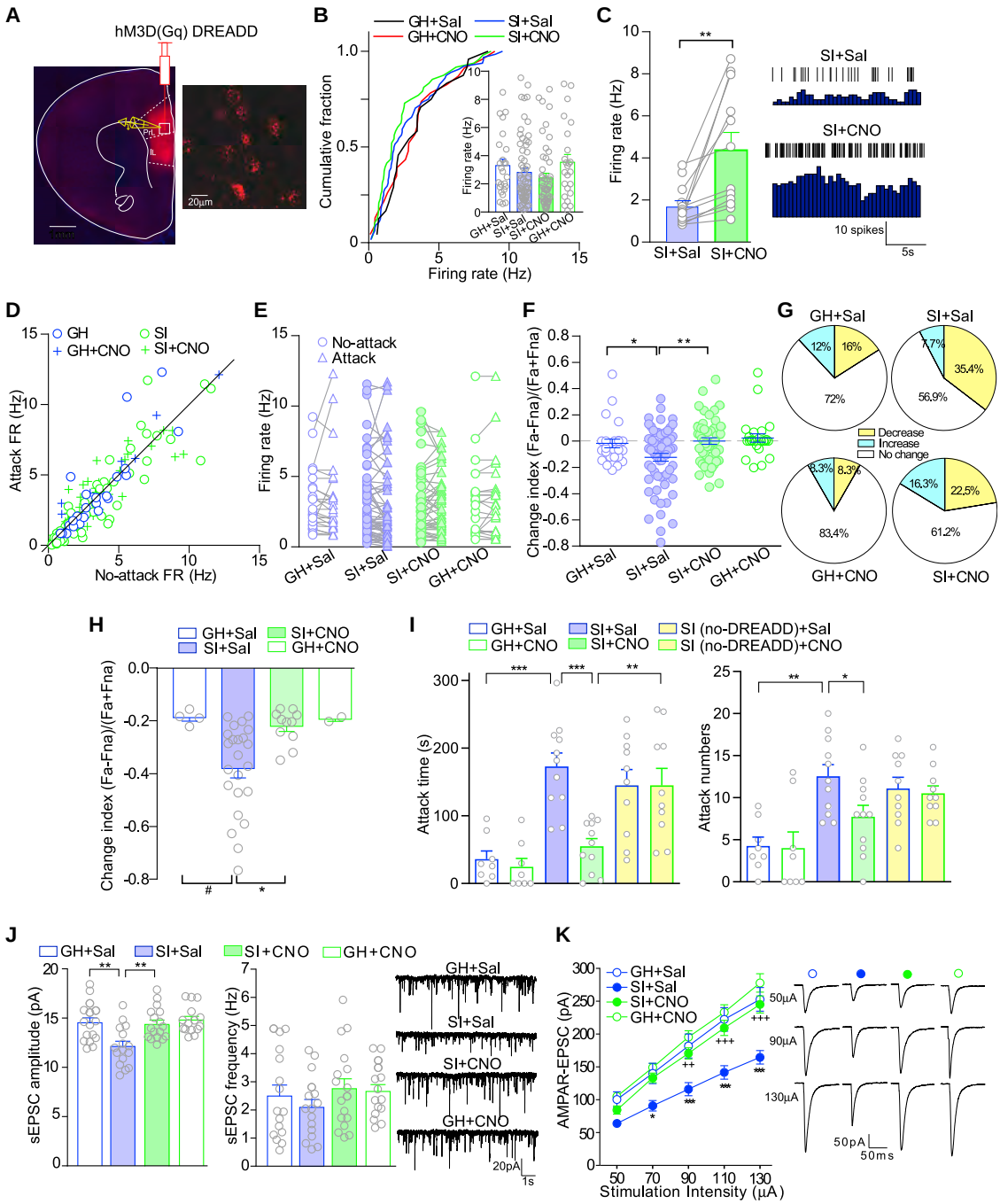

Figure 3. In SI males, chemogenetic stimulation of PFC pyramidal neurons elevates *in vivo* spike activity and attenuates aggression in the RI test

(A) Immunofluorescent image of a brain slice from a male mouse showing the expression of hM3D(Gq)-DREADD (mCherry-tagged) in mPFC. PrL, prelimbic; IL, infralimbic. The electrode demonstrates the recording site of mPFC either *in vivo* (B–G) or *in vitro* (J and K).

(B) Distribution plots of the average firing frequency of recorded PN units at baseline (3 min before the RI test) in saline- or CNO-injected (3 mg/kg, i.p.) GH and SI males with prior infection of hM3Dq in mPFC (n = 25–65 units, 6–8 mice in each group).

(C) Bar graphs of the average firing rate of the subpopulation of PN units activated by CNO from SI males (n = 12 units, 8 mice; p = 0.002, paired t test). Inset: representative raster plot and histogram of spikes of a PN unit before (top) and after CNO administration (bottom).

(D and E) Scatterplots of the firing rates of all PN units during attack against no-attack epochs in the RI test of saline- or CNO-injected GH or SI males (hM3Dq in mPFC).

(F) Scatterplots of attack-associated firing rate change index (CI) of all PN units ($F_{[1,\ 159]\ treatment}$ = 6.0, p = 0.02, two-way ANOVA).

(legend continued on next page)

To find out the physiological basis of CNO effects on *in vivo* spike activity, we performed *in vitro* whole-cell recordings of synaptic function in PFC slices from saline- or CNO-injected GH and SI males (with hM3Dq in mPFC). As shown in Figure 3J, the amplitude, but not frequency, of spontaneous excitatory postsynaptic currents (sEPSCs) was significantly reduced in PFC PNs of SI males (SI + saline) compared with GH controls (GH + saline), which was restored by CNO treatment (SI + CNO). CNO treatment had long-lasting effects over 4 h (Figure S7). Synaptic strength, as indicated by the input-output curve of EPSCs evoked by a series of stimuli, was also significantly diminished in PFC PNs from SI males, and CNO treatment restored it to the control level (Figure 3K). Taken together, these results indicate that chemogenetic activation of PFC of SI males increases synaptic excitation, blocking the activity loss of a population of PFC PNs in RI tests, which leads to the suppression of aggressive behaviors.

In stressed females, chemogenetic stimulation of PFC facilitates the activation of PFC pyramidal neurons by social stimuli and alleviates social withdrawal behavior

In SI females, having found a link between the blunted activation of PFC PNs by social stimuli and social withdrawal behavior, we next examined whether increasing PFC neuronal activity is capable of enhancing sociability. GH and SI females were injected with hM3Dq into mPFC (Figure 4A), and *in vivo* spike activity of PFC in saline- or CNO-injected mice while performing the SA test was assessed. CNO administration did not significantly alter the baseline firing when all the recorded PN units were counted (Figure 4B), but a subpopulation of PN units from SI females showed significantly elevated activity after CNO administration compared with saline treatment (Figure 4C), confirming the capability of hM3Dq to increase the activity of PFC PNs in SI females.

In SA tests, CNO treatment of SI females normalized the discharge activity during social interaction epochs relative to no-interaction epochs (Figures 4D–4H). The interaction-associated firing rate CI demonstrated a significant increase in PN units from CNO-treated, but not saline-treated, SI females (Figure 4F). Moreover, CNO treatment of SI females balanced the proportion profile, with more PN units showing the increased firing rate during social interaction (SI + saline, 15.8%; SI + CNO, 34.0%) and fewer PN units showing the decreased firing rate during interaction (SI + saline, 19.3%; SI + CNO, 7.6%) (Figure 4G). Further examination of the increased PN units revealed that this cell population in CNO-treated SI females had significantly more enhancement of the firing rate than saline-treated SI females (Figure 4H). Correlating with the increase of PFC neuronal activity by social stimuli in the SI + CNO group, CNO administration also improved the sociability of these mice, as demonstrated by the longer social interaction time in SA tests (Figure 4I). However, in SI females with no-DREADD controls, CNO injection failed to improve the diminished sociability (Figure 4I).

Whole-cell recordings of synaptic function (Figures 4J and 4K) in PFC slices from saline- or CNO-injected GH and SI females (with hM3Dq in mPFC) indicated that the amplitude of spontaneous and evoked EPSC was significantly reduced in PFC PNs of SI females (SI + saline), which was restored by CNO treatment (SI + CNO). These results indicate that chemogenetic activation of PFC of SI females increases synaptic excitation, facilitating the activation of a population of PFC PNs by social stimuli in SA tests, which leads to the alleviation of social withdrawal behavior.

In stressed males, hyperactivity of BLA principal neurons, which results from PFC hypofunction, contributes to elevated aggression

We next explored neural circuits that mediate aggressive behaviors in SI males. Hyper-activated amygdala has been implicated in peripuberty stress-induced aggression (Márquez et al., 2013; Papilloud et al., 2019; Rosell and Siever, 2015; Tóth et al., 2008). PFC regulates emotional behavior via top-down control of BLA (Marek et al., 2019; McGarry and Carter, 2017; Sotres-Bayon and Quirk, 2010) by forming direct excitatory synapses and feedforward inhibitory circuits onto BLA principal neurons (Arruda-Carvalho and Clem, 2014) (Figure 5A), so we examined the involvement of the PFC-to-BLA pathway in SI-induced male aggression.

We first measured the impact of PFC activation on BLA principal neurons. hM3D (Gq) was bilaterally injected into mPFC of control mice, and CNO (5 μM) was applied on BLA slices to stimulate PFC-to-BLA synaptic terminals during patch-clamp recordings of BLA principal neurons. As shown in Figure 5B, bath application of CNO significantly inhibited the synaptic-driven spontaneous action potential (sAP) frequency in BLA principal neurons of SI males. Moreover, CNO significantly increased the frequency of spontaneous inhibitory postsynaptic currents (sIPSCs; Figure 5B), without affecting the frequency of sEPSCs (Figure 5B). This indicates that PFC inputs exert a net inhibitory impact on the activity of BLA principal neurons via the dominant feedforward inhibitory circuits.

Next, we examined the stress-induced alteration of the PFC-to-BLA pathway in males. Compared with GH males, the frequency of sIPSCs in BLA principal neurons of SI males was dramatically decreased, which was largely reversed by activation of PFC (infected with hM3Dq) with CNO (Figure 5C).

(G) Pie graphs showing the proportions of PN units with an increase, a decrease, and no change in firing rate during attack epochs relative to no-attack epochs in saline- or CNO-injected GH or SI males (hM3Dq in mPFC) ($p = 0.1$, chi-square test).

(H) Bar graphs of CI in the subpopulation of decreased PN units from saline- or CNO-injected GH or SI males (hM3Dq in mPFC) ($F_{[1, 36]\ group} = 2.9$, $p = 0.1$, two-way ANOVA).

(I) Bar graphs of aggressive behaviors in RI tests of GH or SI males (hM3Dq or no-DREADD in mPFC) injected with saline or CNO (n = 8–11 mice in each group; attack time: $F_{[5, 52]} = 11.54$, $p < 0.0001$; attack numbers: $F_{[5, 52]} = 6.75$, $p < 0.0001$, one-way ANOVA).

(J and K) Bar graphs of spontaneous EPSCs (sEPSCs; J) and evoked AMPAR-EPSCs (K) in PFC pyramidal neurons from saline- or CNO-injected GH or SI males (hM3Dq in mPFC) (n = 15–17 cells, 3 or 4 mice in each group; sEPSC amplitude: $F_{[1, 60]\ interaction} = 5.0$, $p = 0.029$; eEPSCs: $F_{[3, 59]\ group} = 9.2$, $p < 0.0001$, two-way ANOVA). Inset: representative traces.

#$p < 0.1$, *$p < 0.05$, **$p < 0.01$, and ***$p < 0.001$. All data were presented as means ± SEM. See also Figure S7.

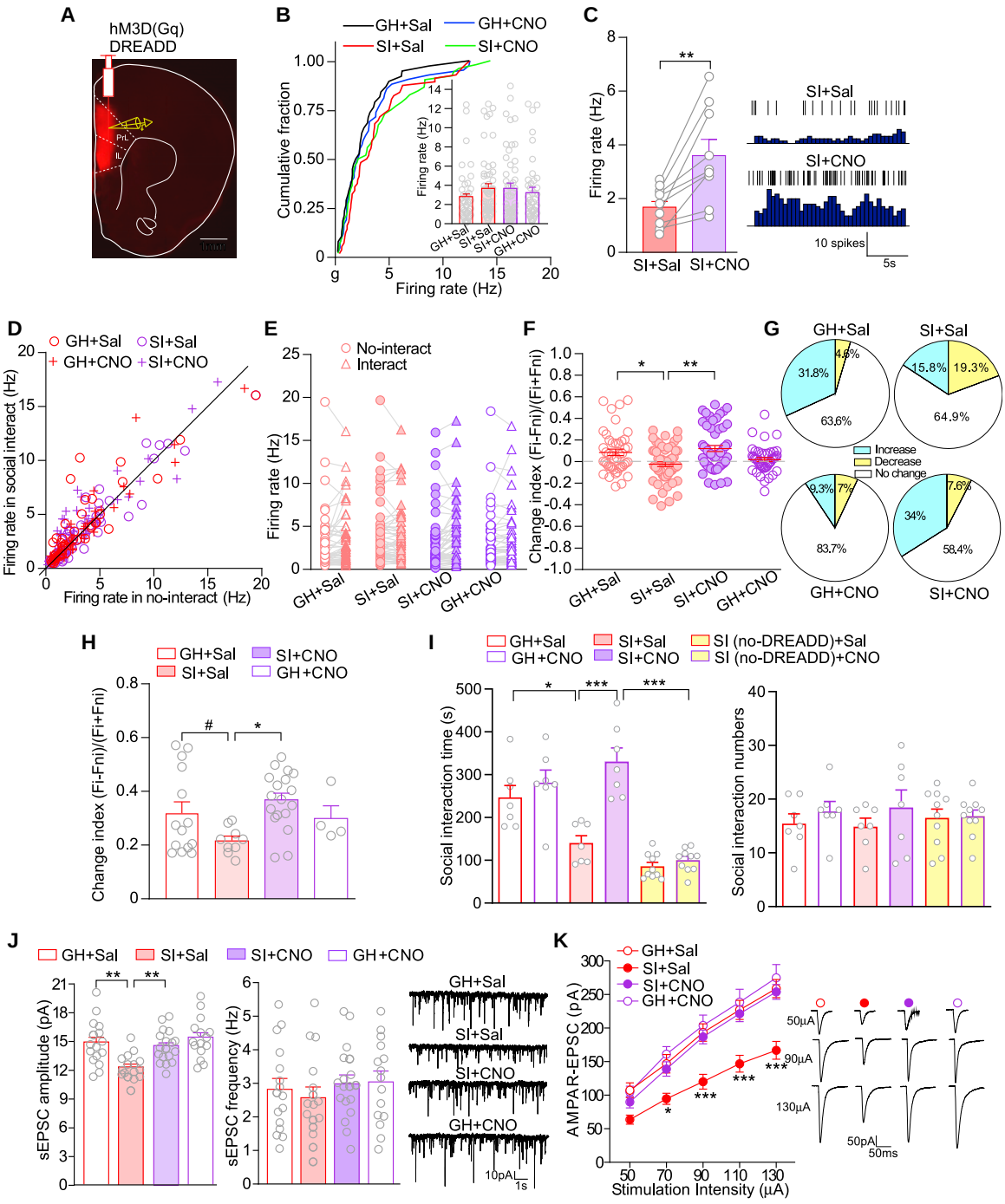

Figure 4. In SI females, chemogenetic stimulation of PFC pyramidal neurons elevates *in vivo* spike activation by social stimuli and enhances sociability in the SA test

(A) Immunofluorescent image of a brain slice from a female mouse showing the expression of hM3D(Gq)-DREADD (mCherry-tagged) in mPFC. The electrode demonstrates the recording site of mPFC either *in vivo* (B–G) or *in vitro* (J and K).

(B) Distribution plots of the average firing frequency of recorded PN units at baseline (5 min before the SA test) in saline- or CNO-injected GH or SI females with prior infection of hM3Dq in mPFC (n = 43–56 units, 6 mice in each group).

(C) Bar graphs of average firing rate of the subpopulation of PN units activated by CNO from SI females (n = 9 units, 6 mice; p = 0.002, paired t test). Inset: representative raster plot and histogram of spikes of a PN unit before (top) and after CNO administration (bottom).

(D and E) Scatterplots of the firing rates of all PN units during social interaction against no-interaction epochs in the SA test of saline- or CNO-injected GH or SI females (hM3Dq in mPFC).

(legend continued on next page)

Concurrently, the frequency of sAP in BLA principal neurons of SI males was elevated, which was partially attenuated by chemogenetic activation of PFC (Figure 5D). These data suggest that chronic isolation stress of males induces BLA disinhibition and hyperactivity, which is caused by PFC hypofunction. In contrast, neuronal activity and synaptic function were not altered in BLA principal neurons from SI females (Figure S4).

Given the hyperactivity of BLA principal neurons in SI males, we next examined the impact of direct inhibition of BLA principal neurons. We injected CaMKII promoter-driven, mCherry-tagged hM4D (Gi) into BLA (Figure 5E) and performed behavioral and electrophysiological experiments on saline- or CNO-injected GH and SI males. In RI tests, CNO treatment reduced aggression, as demonstrated by the smaller number and shorter durations of attacks (Figure 5F). As shown in Figures 5G and 5H, the significantly increased sAP and evoked action potential (eAP) frequencies in BLA principal neurons from SI males (SI + saline) were reversed to control levels by chemogenetic inhibition of BLA (SI + CNO), correlating with the normalization of aggressive behaviors. No significant difference was found in the resting membrane potential (Figure S6A), injected current for sAP (Figure S6B), or input resistance (Figure S6C) from these neurons.

In stressed females, hypoactivity of VTA dopaminergic neurons, which results from diminished PFC inputs, contributes to social withdrawal

We next explored neural circuits that mediate social withdrawal behaviors in SI females. VTA, which is regulated by PFC projections (Sesack and Carr, 2002), plays a central role in motivational and social behaviors (Averbeck and Costa, 2017; Gunaydin et al., 2014; Song et al., 2018) and stress responses (Greenberg et al., 2015; Zhong et al., 2018), so we examined the involvement of the PFC-to-VTA pathway in SI-induced female social withdrawal.

We first manipulated PFC activity with hM3D (Gq) injection and examined the alteration of the PFC-to-VTA pathway in SI females (Figure 6A). We focused on VTA dopaminergic (DA) neurons, which were identified by their pronounced hyperpolarization-activated current (I_h) and pacemaker-like firing (Friedman et al., 2014). As shown in Figure 6B, compared with GH controls (GH + saline), significant decreases in sEPSC amplitude and frequency were found in VTA DA neurons from SI females (SI + saline), which was restored by chemogenetic activation of PFC in CNO-injected SI females (SI + CNO). No significant changes in sIPSC amplitude or frequency were found in VTA DA neurons from SI females (Figure 6C). Moreover, the diminished excitability of VTA DA neurons in SI females was largely recovered by activation of PFC (infected with hM3Dq) with CNO (Figure 6D). No significant changes in synaptic function, neuronal excitability, and I_h were found in VTA DA neurons from SI males (Figure S5).

Given the hypoactivity of VTA DA neurons in SI females, we next examined the impact of direct stimulation of VTA. We injected CaMKII promoter-driven, mCherry-tagged hM3Dq (Gq) into VTA (Figure 6E) and performed electrophysiological and behavioral experiments on saline- or CNO-injected GH and SI females. As shown in Figures 6F–6H, the significantly decreased sEPSC amplitude and frequency and sAP and eAP frequency in VTA DA neurons from SI females were restored by chemogenetic stimulation of VTA (SI + CNO). No significant difference was found in the resting membrane potential (Figure S6C) or input resistance (Figure S6D) from these neurons. Moreover, CNO also reversed the significantly increased I_h amplitude in VTA DA neurons from SI females (Figure 6I). Correlating with the normalization of neuronal activity, CNO treatment significantly enhanced sociability, as demonstrated by the longer social interaction time in SA tests (Figure 6J).

DISCUSSION

Exposure to prolonged stress induces heightened vulnerability to anxiety, depression, and other psychiatric disorders (de Kloet et al., 2005; Fone and Porkess, 2008). Here we show that chronic adolescent isolation stress induces sex-specific behavioral and physiological alterations. Stressed males exhibit escalated aggression, which is correlated with the dampened activity in PFC PNs during attacks of intruders; stressed females show social withdrawal, which is correlated with the blunted activation of PFC PNs by social stimuli. Chemogenetic stimulation of PFC PNs reverses PFC dysfunction and ameliorates behavioral deficits in both stressed males and females. The sexually dimorphic effects of stress are dependent on two distinct target regions of PFC. Hyperactivity of BLA principal neurons is specifically linked to stress-induced male aggression, while hypoactivity of VTA DA neurons is specifically involved in stress-induced female social withdrawal.

In our stress paradigm, the time frame of isolation coincides with the initiation and enhancement of play behavior, a form of non-serious fighting specific to the juvenile/adolescent period, which is essential for preparing for adult life (Pellis and Pellis, 2017). The behavioral results have demonstrated that chronic social isolation causes improper responses. Stressed males easily turn normal social bouts into aggressive attacks within their own territory (RI test). Stressed females have impaired social motivation, as shown by less willingness for engaging in social

(F) Scatterplots of social interaction-associated firing rate change index (CI) of all PN units ($F_{[1,\ 192]\ interaction} = 17.4$, $p < 0.001$, two-way ANOVA).
(G) Pie graphs showing the proportions of PN units with an increase, decrease, and no change of firing rate during social interaction epochs relative to no-interaction epochs in saline- or CNO-injected GH or SI females (hM3Dq in mPFC) ($p = 0.005$, chi-square test).
(H) Bar graphs of CI in the subpopulation of increased PN units in saline- or CNO-injected GH or SI females (hM3Dq in mPFC) ($F_{[1,\ 41]\ interaction} = 4.5$, $p = 0.04$, two-way ANOVA).
(I) Bar graphs of social behaviors in the SA test of GH or SI females (hM3Dq or no-DREADD in mPFC) injected with saline or CNO (n = 7–10 mice in each group; social interaction time: $F_{[5,\ 42]} = 25.46$, $p < 0.0001$, one-way ANOVA).
(J and K) Bar graphs of sEPSCs (J) and evoked AMPAR-EPSCs (K) in PFC pyramidal neurons from saline- or CNO-injected GH or SI females (hM3Dq in mPFC) (sEPSCs: n = 15–18 cells, 4 mice in each group; sEPSC amplitude: $F_{[1,\ 61]\ treatment} = 8.1$, $p = 0.006$; eEPSCs: n = 15–18 cells, 4 mice in each group; $F_{[3,\ 64]\ group} = 8.6$, $p < 0.001$, two-way ANOVA). Inset: representative traces.
# $p < 0.1$, *$p < 0.05$, **$p < 0.01$, and ***$p < 0.001$. All data were presented as means ± SEM. See also Figure S7.

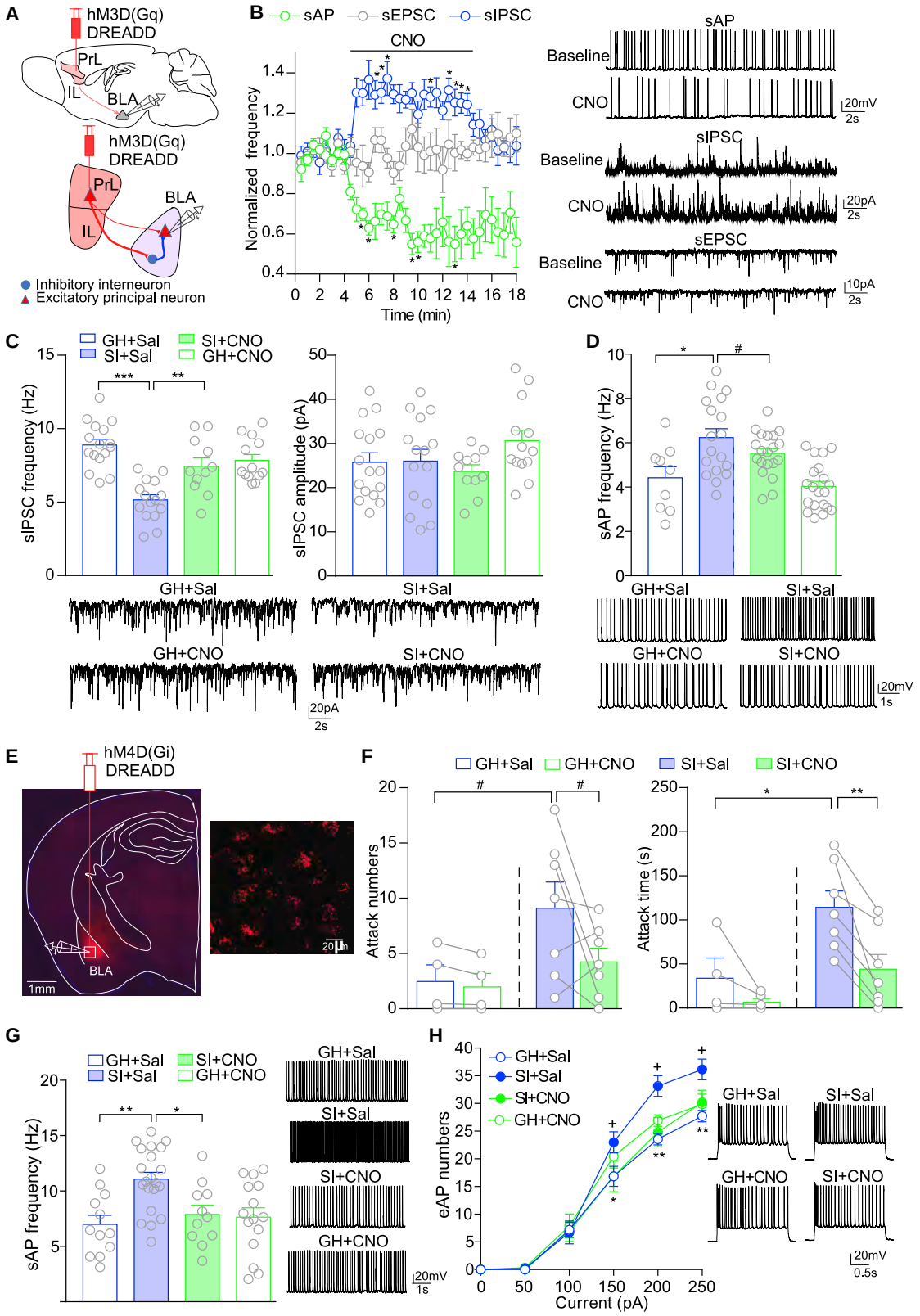

(legend on next page)

interaction (SA test). These behavioral results are largely consistent with prior reports on the sex-specific effects of various stressors (Farrell et al., 2016; Greenberg et al., 2015; Tóth et al., 2008; Wei et al., 2018; Zelikowsky et al., 2018). The RI test is well established to test male aggression, as males tend to show more territorial and social dominance behaviors than females. Although aggression can also be observed in females using RI test, this is mostly observed in lactating dams with male intruders (Hashikawa et al., 2017; Pfaff, 2002). In the present study, we did not find aggressive behaviors in SI females, which may result from the low sensitivity of the RI test for female aggression. Although a decreased social preference was reported in males after 2 week social isolation (Zelikowsky et al., 2018), we have found normal social interaction in the SA test of males subjected to 5 week adolescent isolation stress. Different isolation procedures and behavioral tests may lead to different results.

What drives the behavioral abnormality in stressed animals? We first focused on PFC, a key region implicated in the inhibitory control of emotional outbursts, including aggression and violence (Davidson et al., 2000; Nelson and Trainor, 2007). In humans, PFC lesions cause the onset of impulsive behaviors, and violent patients exhibit decreased PFC activity (Anderson et al., 1999; Brower and Price, 2001). In animals, optogenetic silencing of mPFC neurons causes an escalation of aggressive behavior, while optogenetic activation of mPFC excitatory neurons inhibits aggression (Takahashi et al., 2014). PFC is also highly implicated in sociability because of its enhanced activity during social interaction (Jennings et al., 2019; Kim et al., 2015; Lee et al., 2016; Minami et al., 2017). In isolation stressed animals, PFC neurons have attenuated c-Fos induction by social interaction (Wall et al., 2012). Our *in vivo* recording of behaving animals and chemogenetic studies suggest that the heightened aggressive behavior in stressed males is driven by the attenuation of PFC PN activity, while the social withdrawal in stressed females is driven by the loss of enhancement of PFC PN activity by social stimuli.

PFC exerts its pleiotropic effects by controlling distinct subcortical regions. One of the PFC-interacting regions is the amygdala, which plays a determinant role in threat detection and fear responses (Fanning et al., 2017; McCloskey et al., 2016; Miller et al., 2019). Anatomic studies have found that each of the rat PFC subregions has a distinctive projection to the amygdala, with PL projecting mainly to BLA (Mcdonald et al., 1996). BLA projects to the central amygdala, which provides the major output of the amygdala complex to control fear and emotional responses. Activation of the amygdala promotes aggression (Flanigan and Russo, 2019; Hong et al., 2014), a kind of inappropriate emotional reactivity to perceived social threats and poor impulse control (Flanigan and Russo, 2019). Our electrophysiological data indicate that stressed males engaged in impulsive aggression have abnormal brain function in the limbic system: hyper-responsivity in emotional circuitry such as the amygdala and hypo-responsivity in emotion regulation circuitry such as the PFC, which is consistent with fMRI studies of human subjects (Fanning et al., 2017). Using DREADD to activate PL axon terminals in BLA, we have observed the reduced excitability and increased inhibitory synaptic currents on BLA principal neurons, suggesting that PFC inputs suppress the activity of BLA principal neurons via feedforward inhibition (Wei et al., 2018). Consistently, *in vivo* intracellular recordings demonstrate that PFC stimulation inhibits BLA projection neurons, which is attributable to the recruitment of inhibitory interneurons (Rosenkranz and Grace, 2002). The mitigation of aggression by chemogenetic activation of PFC or inhibition of BLA suggests the important role of the PFC-to-BLA pathway in male stress responses. However, only pathway-specific chemo-/optogenetics in behaving animals can conclusively establish the PFC-to-BLA or PFC-to-VTA pathways as the causal link to the observed behavioral deficits. We also do not exclude the potential involvement of other PFC-connected pathways in aggression, such as hypothalamic regions, which have been strongly implicated in the control of aggression (Falkner et al., 2016; Golden et al., 2019; Hashikawa et al., 2016; Nelson and Trainor, 2007).

To find out PFC-interacting subcortical regions involved in social withdrawal behavior in stressed females, we focused on VTA, because VTA activity dynamics is found to encode and predict key features of social interaction (Gunaydin and Deisseroth, 2014). Deficits in the postnatal development of excitatory transmission onto VTA DA neurons lead to sociability deficits (Bariselli

Figure 5. In SI males, BLA principal neurons are overactive, which is reversed by chemogenetic stimulation of PFC pyramidal neurons, and chemogenetic inhibition of BLA mitigates aggression in the RI test

(A) Schematics showing viral injection into the mPFC and recording in the basolateral amygdala (BLA) (left), and viral-infected mPFC pyramidal neurons project to both principal neurons and GABAergic interneurons in BLA (right).

(B) Plots showing normalized sAP, sIPSC, and sEPSC frequency before (baseline), during (CNO), and after (wash) bath application of CNO (5 μM) in BLA principal neurons from SI males with prior infection of hM3Dq in mPFC (n = 5–6 cells, three mice in each group; sAP: F = 11.1, p = 0.0001; sIPSC: F = 3.6, p = 0.04; one-way rmANOVA).

(C) Bar graphs showing sIPSCs in BLA principal neurons from saline- or CNO-injected GH and SI males (hM3Dq in mPFC) (n = 11–16 cells, four mice in each group; sIPSC frequency: $F_{[1, 51]\ interaction} = 15.3$, $p < 0.001$, two-way ANOVA).

(D) Bar graphs showing the frequency of synaptic-driven sAP in BLA principal neurons from saline- or CNO-injected GH or SI males (hM3Dq in mPFC) (n = 9–20 cells, four or five mice in each group; $F_{[1, 51]\ group} = 11.9$, $p = 0.001$, two-way ANOVA).

(E) Immunofluorescent image of a brain slice from a male mouse showing the expression of (Gi)-DREADD (mCherry-tagged) in BLA.

(F) Bar graphs showing aggressive behaviors of GH and SI males (hM4Di in BLA) in the RI tests before (saline) and after CNO injection (n = 4–7 mice in each group; attack numbers: $F_{[1, 9]\ group} = 4.3$, $p = 0.07$; attack time: $F_{[1, 9]\ treatment} = 15.2$, $p = 0.004$; two-way rmANOVA).

(G and H) Plots showing the frequency of sAP (G) and eAP (H) in BLA principal neurons from saline- or CNO-injected GH and SI males (hM4Di in BLA) (sAP: n = 11–21 cells, four or five mice in each group, $F_{[1, 55]\ interaction} = 5.8$, $p = 0.02$, two-way ANOVA; eAP: n = 8–14 cells, four mice in each group, $F_{[3, 36]\ group} = 3.5$, $p = 0.02$, two-way rmANOVA).

Inset (B–D, G, and H): representative traces. # $p \leq 0.1$, *$p < 0.05$, **$p < 0.01$, and ***$p < 0.001$. All data were presented as means ± SEM. See also Figures S3, S4, and S6.

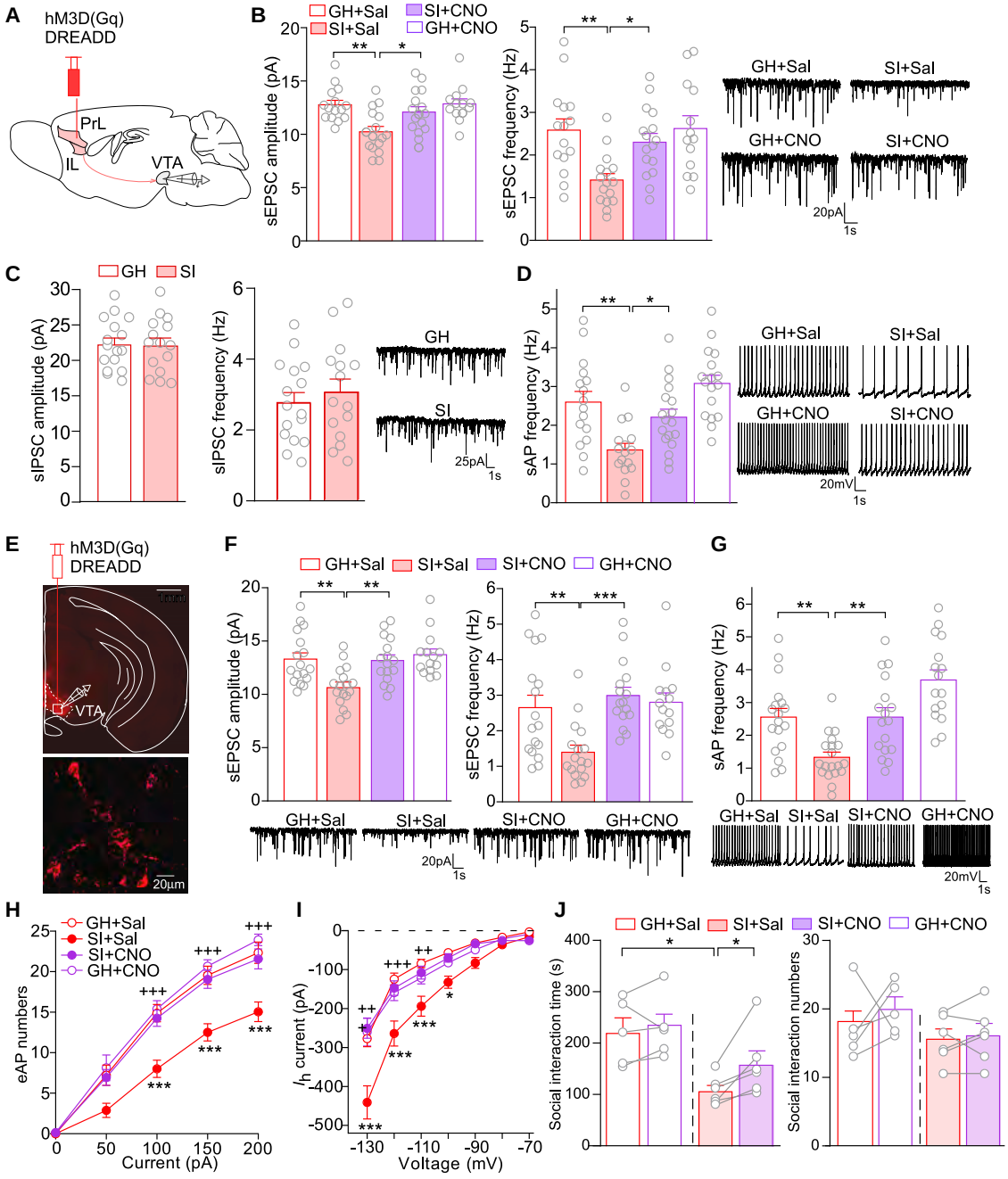

Figure 6. In SI females, VTA dopaminergic (DA) neurons are hypoactive, which is reversed by chemogenetic stimulation of PFC pyramidal neurons, and chemogenetic activation of VTA enhances sociability in the SA test

(A) Schematic showing viral injection into the mPFC and recording in the ventral tegmental area (VTA) for (B)–(F).

(B) Bar graphs showing sEPSCs in VTA putative DA neurons from saline- or CNO-injected GH or SI females with prior infection of hM3Dq in mPFC (n = 13–16 cells, four mice in each group; sEPSC amplitude: $F_{[1,\ 56]\ interaction} = 3.5$, $p = 0.07$; sEPSC frequency: $F_{[1,\ 56]\ interaction} = 3.4$, $p = 0.07$; two-way ANOVA).

(C) Bar graphs of sIPSCs in VTA DA neurons from GH and SI females (n = 15 or 16 cells, three mice each group).

(D) Plots of sAP in VTA DA neurons from saline- or CNO-injected GH or SI females (hM3Dq in mPFC) (n = 16–18 cells, five or six mice in each group; $F_{[1,\ 63]\ treatment} = 9.0$, $p = 0.004$).

(E) Immunofluorescent image of a brain slice from a female mouse showing the expression of hM3D(Gq)-DREADD (mCherry-tagged) and recording in VTA for (H)–(L).

(F–I) Plots of sEPSC (F), sAP (G), eAP (H), and I_h (I) in VTA DA neurons from saline- or CNO-injected GH or SI females with prior infection of hM3Dq in VTA (n = 14–23 cells, four to six mice in each group; sEPSC amplitude: $F_{[1,\ 60]\ interaction} = 3.7$, $p = 0.06$; sEPSC frequency: $F_{[1,\ 60]\ interaction} = 7.1$, $p = 0.01$; sAP frequency: $F_{[1,\ 66]\ treatment} = 21.1$, $p < 0.0001$, two-way ANOVA; eAP number: $F_{[3,\ 66]\ group} = 12.4$, $p < 0.0001$; I_h: $F_{[3,\ 77]\ group} = 8.7$, $p < 0.0001$, two-way rmANOVA).

(legend continued on next page)

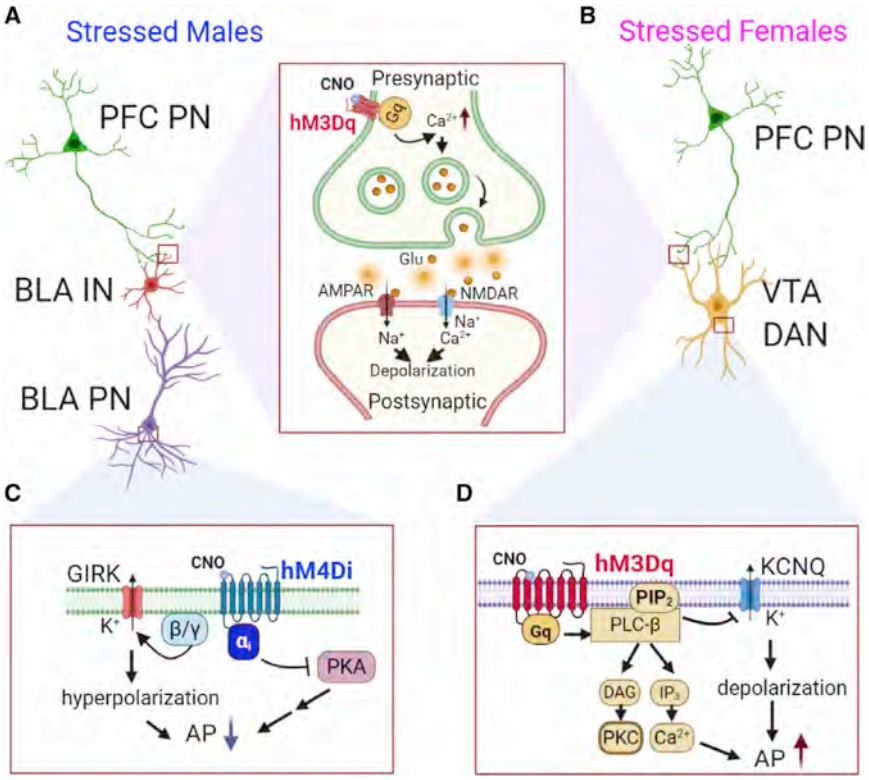

Figure 7. Schematic diagrams showing the mechanisms underlying chemogenetic modulation of neuronal circuits in social isolation (SI) stressed males and females

(A and B) Activation of Gq DREADD at presynaptic terminals of PFC pyramidal neurons (PNs) increases Ca^{2+} concentration and facilitates glutamate (Glu) release, which activates postsynaptic AMPARs and NMDARs, leading to the increased stimulation of BLA interneurons (INs) and feedforward inhibition of BLA principal neurons (PNs) in SI males (A) and the increased stimulation of VTA DA neurons (DANs) in SI females (B).

(C) Activation of Gi DREADD in BLA principal neurons (PNs) of SI males activates G protein-coupled inwardly rectifying potassium channels (GIRKs) and blocks the PKA pathway, leading to the suppression of BLA principal neuronal activity.

(D) Activation of Gq DREADD in VTA DA neurons (DANs) of SI females increases intracellular Ca^{2+} levels and prevents K^+ outflux through KCNQ channels via the hydrolysis of PIP_2, leading to the elevation of VTA DA neuronal activity.

et al., 2016). Chronic mild stress leads to the reduction of action potential firing of VTA DA neurons (Chang and Grace, 2014), while social defeat stress induces hyperactivity of VTA DA neurons in susceptible mice (Friedman et al., 2014). In isolation stressed females, we have detected hypoactivity of VTA DA neurons, which is likely caused by the diminished excitatory inputs from PFC onto these neurons. The amelioration of social withdrawal by chemogenetic activation of PFC or activation of VTA suggests the important role of PFC to VTA pathway in female stress responses. In contrast to the reported hyperactivity of VTA DA neurons in susceptible male mice after social defeat stress (Friedman et al., 2014), here we did not find activity changes in VTA DA neurons of SI males. Different stressors are likely to induce a different set of molecular and physiological adaptations (Fox and Lobo, 2019).

In this study, we used Gq and Gi DREADDs as tools to manipulate neuronal activity in specific regions, consistent with their general utility in other studies (Roth, 2016). Activation of Gq DREADD (injected into PFC of SI animals) triggers PLC/Ca^{2+}-mediated increase of presynaptic transmitter release, leading to the increased activation of BLA interneurons and feedforward inhibition of BLA principal neurons in SI males (Figure 7A), as well as the increased activation of VTA dopamine neurons in SI females (Figure 7B). Activation of Gi DREADD (injected into BLA of SI males) attenuated BLA principal neuronal activity, probably through Gβ/γ-mediated opening of G protein-coupled inwardly rectifying potassium channels (GIRK) and inhibition of PKA pathway (Aldrin-Kirk and Björklund, 2019) (Figure 7C). Activation of Gq DREADD (injected into VTA of SI females) elevated VTA DA neuronal activity, probably through the increase of intracellular Ca^{2+} and the blockade of K^+ outflux through KCNQ channels via the hydrolysis of PIP_2 (Zaydman and Cui, 2014) (Figure 7D). Furthermore, the modulatory role of DREADD on the hyperpolarization-activated cyclic nucleotide-gated channel (HCN) (Cheng et al., 2019; Aldrin-Kirk et al., 2016) may contribute to the effect of Gq DREADD on I_h in VTA DA neurons.

Most of experiments in this study used i.p. injection of CNO at 3 mg/kg, a dose that effectively activates DREADD *in vivo* without unspecific behavioral effects in mice (Jendryka et al., 2019). We found minimal effects of CNO injection on GH control animals, which is in agreement with prior reports on behaviors (Aldrin-Kirk et al., 2016; Chen et al., 2020; Cheng et al., 2017; Liu et al., 2014a; Sharma et al., 2020; Wang et al., 2018; Wei et al., 2018) and electrophysiology (Cheng et al., 2017; Wang et al., 2018; Wei et al., 2018). Systematic application of CNO (3 mg/kg, i.p.) reaches the brain at ~25 nM, which is much lower than the doses usually used *in vitro* (e.g., 5 μM) (Jendryka et al., 2019). We speculate that this low dose of CNO preferably works in abnormal conditions when GPCR signaling and neuronal activity are compromised. Once the dose is high enough, CNO injection also regulates neuronal activity in control animals, even inducing seizures (Alexander et al., 2009).

(J) Bar graphs of social behaviors in saline- or CNO-injected GH or SI females (hM3Dq in VTA) in the SA test (n = 5 or 6 mice in each group; social interaction time: $F_{[1,\ 9]\ group} = 8.6$, $p = 0.02$, two-way rmANOVA).

Inset (B–D, F, and G): representative traces. *$p < 0.05$, **$p < 0.01$, and ***$p < 0.001$. All data were presented as means ± SEM. See also Figures S3, S5, and S6.

One important question is how DREADD normalizes the compromised GPCR signaling in SI mice. It is known that catecholamines such as dopamine and noradrenaline, which exert "inverted U-shaped" influences on PFC physiology and function, are disturbed by stress (Arnsten, 2009). Prior studies show that stress-induced aberrations of these receptors alter calcium-cAMP signaling, leading to the abnormal gating of ion channels, the reduced firing of PFC neurons, and the impaired top-down control of emotional processes (Arnsten and Wang, 2012). Future studies will address the detailed mechanisms of Gq and Gi DREADD in the PFC, BLA, and VTA circuits of males and females exposed to chronic isolation stress.

Collectively, we have interrogated brain regions and cell types governing sex-specific effects of adolescent isolation stress: heightened aggression in males and social withdrawal in females. We demonstrate that these complex behavioral changes are likely the result of aberrant PFC activity and the altered top-down control of divergent neural systems, including BLA and VTA. Understanding the functional connectivity and behavioral roles of these neural circuitry will aid in the development of effective treatments for stress-related disorders.

STAR★METHODS

Detailed methods are provided in the online version of this paper and include the following:

- KEY RESOURCES TABLE
- RESOURCE AVAILABILITY
  - Lead contact
  - Materials availability
  - Data and code availability
- EXPERIMENTAL MODEL AND SUBJECT DETAILS
  - Animal subjects
- METHOD DETAILS
  - Social isolation stress
  - Behavioral testing
  - Resident-intruder (RI) test
  - Social approach (SA) test
  - Viral vectors and injection
  - *In vivo* recording
  - Surgical implantation of the electrode array
  - Electrophysiological recording of behaving mice
  - Spike sorting
  - Unit classification and firing rate analysis
  - Whole-cell recording in brain slices
  - Voltage-clamp recording of EPSC, IPSC and I_h
  - Current-clamp recording of spontaneous AP and evoked AP
  - Imaging
- QUANTIFICATION AND STATISTICAL ANALYSIS

SUPPLEMENTAL INFORMATION

Supplemental information can be found online at https://doi.org/10.1016/j.celrep.2021.108874.

ACKNOWLEDGMENTS

We thank Freddy Zhang, Dr. Luye Qin, and Xiaoqing Chen for excellent technical support. This work was supported by a grant from the National Institutes of Health, United States (MH108842) to Z.Y.

AUTHOR CONTRIBUTIONS

T.T. designed experiments, performed behavioral and electrophysiological (*in vivo* and *in vitro*) experiments, analyzed data, and wrote the paper. W.W. performed *in vitro* electrophysiological experiments and analyzed data. T.L. performed *in vivo* electrophysiological experiments and analyzed data. P.Z. performed some *in vitro* electrophysiological experiments and analyzed data. M.C.-G. performed some behavioral assays. X.T. supervised *in vivo* electrophysiological experiments. Z.Y. designed experiments, supervised the project, and wrote the paper.

DECLARATION OF INTERESTS

The authors declare no competing interests.

Received: May 28, 2020
Revised: September 9, 2020
Accepted: February 25, 2021
Published: March 23, 2021

REFERENCES

Aldrin-Kirk, P., and Björklund, T. (2019). Practical considerations for the use of DREADD and other chemogenetic receptors to regulate neuronal activity in the mammalian brain. Methods Mol. Biol. *1937*, 59–87.

Aldrin-Kirk, P., Heuer, A., Wang, G., Mattsson, B., Lundblad, M., Parmar, M., and Björklund, T. (2016). DREADD modulation of transplanted DA neurons reveals a novel parkinsonian dyskinesia mechanism mediated by the serotonin 5-HT6 receptor. Neuron *90*, 955–968.

Alexander, G.M., Rogan, S.C., Abbas, A.I., Armbruster, B.N., Pei, Y., Allen, J.A., Nonneman, R.J., Hartmann, J., Moy, S.S., Nicolelis, M.A., et al. (2009). Remote control of neuronal activity in transgenic mice expressing evolved G protein-coupled receptors. Neuron *63*, 27–39.

Anderson, S.W., Bechara, A., Damasio, H., Tranel, D., and Damasio, A.R. (1999). Impairment of social and moral behavior related to early damage in human prefrontal cortex. Nat. Neurosci. *2*, 1032–1037.

Arnsten, A.F. (2009). Stress signalling pathways that impair prefrontal cortex structure and function. Nat Rev Neurosci *10*, 410–422.

Arnsten, A.F., Wang, M.J., and Paspalas, C.D. (2012). Neuromodulation of thought: flexibilities and vulnerabilities in prefrontal cortical network synapses. Neuron *76*, 223–239.

Arruda-Carvalho, M., and Clem, R.L. (2014). Pathway-selective adjustment of prefrontal-amygdala transmission during fear encoding. J. Neurosci. *34*, 15601–15609.

Averbeck, B.B., and Costa, V.D. (2017). Motivational neural circuits underlying reinforcement learning. Nat. Neurosci. *20*, 505–512.

Bale, T.L., and Epperson, C.N. (2015). Sex differences and stress across the lifespan. Nat. Neurosci. *18*, 1413–1420.

Bariselli, S., Tzanoulinou, S., Glangetas, C., Prévost-Solié, C., Pucci, L., Viguié, J., Bezzi, P., O'Connor, E.C., Georges, F., Lüscher, C., and Bellone, C. (2016). SHANK3 controls maturation of social reward circuits in the VTA. Nat. Neurosci. *19*, 926–934.

Brower, M.C., and Price, B.H. (2001). Neuropsychiatry of frontal lobe dysfunction in violent and criminal behaviour: a critical review. J. Neurol. Neurosurg. Psychiatry *71*, 720–726.

Burke, A.R., McCormick, C.M., Pellis, S.M., and Lukkes, J.L. (2017). Impact of adolescent social experiences on behavior and neural circuits implicated in mental illnesses. Neurosci. Biobehav. Rev. *76* (*Pt B*), 280–300.

Chang, C.H., and Grace, A.A. (2014). Amygdala-ventral pallidum pathway decreases dopamine activity after chronic mild stress in rats. Biol. Psychiatry *76*, 223–230.

Chen, P., Lou, S., Huang, Z.H., Wang, Z., Shan, Q.H., Wang, Y., Yang, Y., Li, X., Gong, H., Jin, Y., et al. (2020). Prefrontal cortex corticotropin-releasing factor neurons control behavioral style selection under challenging situations. Neuron *106*, 301–315.e7.

Cheng, J., Liu, A., Shi, M.Y., and Yan, Z. (2017). Disrupted glutamatergic transmission in prefrontal cortex contributes to behavioral abnormality in an animal model of ADHD. Neuropsychopharmacology *42*, 2096–2104.

Cheng, J., Umschweif, G., Leung, J., Sagi, Y., and Greengard, P. (2019). HCN2 channels in cholinergic interneurons of nucleus accumbens shell regulate depressive behaviors. Neuron *101*, 662–672.e5.

Coccaro, E.F., McCloskey, M.S., Fitzgerald, D.A., and Phan, K.L. (2007). Amygdala and orbitofrontal reactivity to social threat in individuals with impulsive aggression. Biol. Psychiatry *62*, 168–178.

Coccaro, E.F., Sripada, C.S., Yanowitch, R.N., and Phan, K.L. (2011). Corticolimbic function in impulsive aggressive behavior. Biol. Psychiatry *69*, 1153–1159.

Davidson, R.J., Putnam, K.M., and Larson, C.L. (2000). Dysfunction in the neural circuitry of emotion regulation—a possible prelude to violence. Science *289*, 591–594.

de Kloet, E.R., Joëls, M., and Holsboer, F. (2005). Stress and the brain: from adaptation to disease. Nat. Rev. Neurosci. *6*, 463–475.

Diehl, M.M., Bravo-Rivera, C., Rodriguez-Romaguera, J., Pagan-Rivera, P.A., Burgos-Robles, A., Roman-Ortiz, C., and Quirk, G.J. (2018). Active avoidance requires inhibitory signaling in the rodent prelimbic prefrontal cortex. eLife *7*, e34657.

Falkner, A.L., Grosenick, L., Davidson, T.J., Deisseroth, K., and Lin, D. (2016). Hypothalamic control of male aggression-seeking behavior. Nat. Neurosci. *19*, 596–604.

Fanning, J.R., Keedy, S., Berman, M.E., Lee, R., and Coccaro, E.F. (2017). Neural correlates of aggressive behavior in real time: a review of fMRI studies of laboratory reactive aggression. Curr. Behav. Neurosci. Rep. *4*, 138–150.

Farrell, M.R., Sengelaub, D.R., and Wellman, C.L. (2013). Sex differences and chronic stress effects on the neural circuitry underlying fear conditioning and extinction. Physiol. Behav. *122*, 208–215.

Farrell, M.R., Holland, F.H., Shansky, R.M., and Brenhouse, H.C. (2016). Sex-specific effects of early life stress on social interaction and prefrontal cortex dendritic morphology in young rats. Behav. Brain Res. *310*, 119–125.

Flanigan, M.E., and Russo, S.J. (2019). Recent advances in the study of aggression. Neuropsychopharmacology *44*, 241–244.

Fone, K.C., and Porkess, M.V. (2008). Behavioural and neurochemical effects of post-weaning social isolation in rodents-relevance to developmental neuropsychiatric disorders. Neurosci. Biobehav. Rev. *32*, 1087–1102.

Fox, M.E., and Lobo, M.K. (2019). The molecular and cellular mechanisms of depression: a focus on reward circuitry. Mol. Psychiatry *24*, 1798–1815.

Friedman, A.K., Walsh, J.J., Juarez, B., Ku, S.M., Chaudhury, D., Wang, J., Li, X., Dietz, D.M., Pan, N., Vialou, V.F., et al. (2014). Enhancing depression mechanisms in midbrain dopamine neurons achieves homeostatic resilience. Science *344*, 313–319.

Fries, A.B., Shirtcliff, E.A., and Pollak, S.D. (2008). Neuroendocrine dysregulation following early social deprivation in children. Dev. Psychobiol. *50*, 588–599.

Gold, P.W. (2015). The organization of the stress system and its dysregulation in depressive illness. Mol. Psychiatry *20*, 32–47.

Golden, S.A., Jin, M., and Shaham, Y. (2019). Animal models of (or for) aggression reward, addiction, and relapse: behavior and circuits. J. Neurosci. *39*, 3996–4008.

Greenberg, G.D., Steinman, M.Q., Doig, I.E., Hao, R., and Trainor, B.C. (2015). Effects of social defeat on dopamine neurons in the ventral tegmental area in male and female California mice. Eur. J. Neurosci. *42*, 3081–3094.

Gunaydin, L.A., and Deisseroth, K. (2014). Dopaminergic dynamics contributing to social behavior. Cold Spring Harb. Symp. Quant. Biol. *79*, 221–227.

Gunaydin, L.A., Grosenick, L., Finkelstein, J.C., Kauvar, I.V., Fenno, L.E., Adhikari, A., Lammel, S., Mirzabekov, J.J., Airan, R.D., Zalocusky, K.A., et al. (2014). Natural neural projection dynamics underlying social behavior. Cell *157*, 1535–1551.

Haller, J., Harold, G., Sandi, C., and Neumann, I.D. (2014). Effects of adverse early-life events on aggression and anti-social behaviours in animals and humans. J. Neuroendocrinol. *26*, 724–738.

Hashikawa, K., Hashikawa, Y., Falkner, A., and Lin, D. (2016). The neural circuits of mating and fighting in male mice. Curr. Opin. Neurobiol. *38*, 27–37.

Hashikawa, K., Hashikawa, Y., Tremblay, R., Zhang, J., Feng, J.E., Sabol, A., Piper, W.T., Lee, H., Rudy, B., and Lin, D. (2017). Esr1^{+} cells in the ventromedial hypothalamus control female aggression. Nat. Neurosci. *20*, 1580–1590.

Heim, C., and Nemeroff, C.B. (2001). The role of childhood trauma in the neurobiology of mood and anxiety disorders: preclinical and clinical studies. Biol. Psychiatry *49*, 1023–1039.

Hiser, J., and Koenigs, M. (2018). The multifaceted role of the ventromedial prefrontal cortex in emotion, decision making, social cognition, and psychopathology. Biol. Psychiatry *83*, 638–647.

Hodes, G.E., Pfau, M.L., Purushothaman, I., Ahn, H.F., Golden, S.A., Christoffel, D.J., Magida, J., Brancato, A., Takahashi, A., Flanigan, M.E., et al. (2015). Sex differences in nucleus accumbens transcriptome profiles associated with susceptibility versus resilience to subchronic variable stress. J. Neurosci. *35*, 16362–16376.

Hong, W., Kim, D.W., and Anderson, D.J. (2014). Antagonistic control of social versus repetitive self-grooming behaviors by separable amygdala neuronal subsets. Cell *158*, 1348–1361.

Ingalhalikar, M., Smith, A., Parker, D., Satterthwaite, T.D., Elliott, M.A., Ruparel, K., Hakonarson, H., Gur, R.E., Gur, R.C., and Verma, R. (2014). Sex differences in the structural connectome of the human brain. Proc. Natl. Acad. Sci. U S A *111*, 823–828.

Jendryka, M., Palchaudhuri, M., Ursu, D., van der Veen, B., Liss, B., Kätzel, D., Nissen, W., and Pekcec, A. (2019). Pharmacokinetic and pharmacodynamic actions of clozapine-N-oxide, clozapine, and compound 21 in DREADD-based chemogenetics in mice. Sci. Rep. *9*, 4522.

Jennings, J.H., Kim, C.K., Marshel, J.H., Raffiee, M., Ye, L., Quirin, S., Pak, S., Ramakrishnan, C., and Deisseroth, K. (2019). Interacting neural ensembles in orbitofrontal cortex for social and feeding behaviour. Nature *565*, 645–649.

Kim, Y., Venkataraju, K.U., Pradhan, K., Mende, C., Taranda, J., Turaga, S.C., Arganda-Carreras, I., Ng, L., Hawrylycz, M.J., Rockland, K.S., et al. (2015). Mapping social behavior-induced brain activation at cellular resolution in the mouse. Cell Rep. *10*, 292–305.

Koolhaas, J.M., Coppens, C.M., de Boer, S.F., Buwalda, B., Meerlo, P., and Timmermans, P.J. (2013). The resident-intruder paradigm: a standardized test for aggression, violence and social stress. J. Vis. Exp. (*77*), e4367.

Labonté, B., Engmann, O., Purushothaman, I., Menard, C., Wang, J., Tan, C., Scarpa, J.R., Moy, G., Loh, Y.E., Cahill, M., et al. (2017). Sex-specific transcriptional signatures in human depression. Nat. Med. *23*, 1102–1111.

Lee, E., Rhim, I., Lee, J.W., Ghim, J.W., Lee, S., Kim, E., and Jung, M.W. (2016). Enhanced neuronal activity in the medial prefrontal cortex during social approach behavior. J. Neurosci. *36*, 6926–6936.

Liston, C., McEwen, B.S., and Casey, B.J. (2009). Psychosocial stress reversibly disrupts prefrontal processing and attentional control. Proc. Natl. Acad. Sci. U S A *106*, 912–917.

Liu, D., Gu, X., Zhu, J., Zhang, X., Han, Z., Yan, W., Cheng, Q., Hao, J., Fan, H., Hou, R., et al. (2014a). Medial prefrontal activity during delay period contributes to learning of a working memory task. Science *346*, 458–463.

Liu, T., Bai, W., Yi, H., Tan, T., Wei, J., Wang, J., and Tian, X. (2014b). Functional connectivity in a rat model of Alzheimer's disease during a working memory task. Curr. Alzheimer Res. *11*, 981–991.

Liu, T., Bai, W., Xia, M., and Tian, X. (2018). Directional hippocampal-prefrontal interactions during working memory. Behav. Brain Res. *338*, 1–8.

Lupien, S.J., McEwen, B.S., Gunnar, M.R., and Heim, C. (2009). Effects of stress throughout the lifespan on the brain, behaviour and cognition. Nat. Rev. Neurosci. *10*, 434–445.

Maffei, A., and Turrigiano, G.G. (2008). Multiple modes of network homeostasis in visual cortical layer 2/3. J. Neurosci. *28*, 4377–4384.

Maffei, A., Nelson, S.B., and Turrigiano, G.G. (2004). Selective reconfiguration of layer 4 visual cortical circuitry by visual deprivation. Nat. Neurosci. *7*, 1353–1359.

Malkesman, O., Maayan, R., Weizman, A., and Weller, A. (2006). Aggressive behavior and HPA axis hormones after social isolation in adult rats of two different genetic animal models for depression. Behav. Brain Res. *175*, 408–414.

Marek, R., Sun, Y., and Sah, P. (2019). Neural circuits for a top-down control of fear and extinction. Psychopharmacology (Berl.) *236*, 313–320.

Marín, O. (2016). Developmental timing and critical windows for the treatment of psychiatric disorders. Nat. Med. *22*, 1229–1238.

Márquez, C., Poirier, G.L., Cordero, M.I., Larsen, M.H., Groner, A., Marquis, J., Magistretti, P.J., Trono, D., and Sandi, C. (2013). Peripuberty stress leads to abnormal aggression, altered amygdala and orbitofrontal reactivity and increased prefrontal MAOA gene expression. Transl. Psychiatry *3*, e216.

McCloskey, M.S., Phan, K.L., Angstadt, M., Fettich, K.C., Keedy, S., and Coccaro, E.F. (2016). Amygdala hyperactivation to angry faces in intermittent explosive disorder. J. Psychiatr. Res. *79*, 34–41.

Mcdonald, A.J., Mascagni, F., and Guo, L. (1996). Projections of the medial and lateral prefrontal cortices to the amygdala: a Phaseolus vulgaris leucoagglutinin study in the rat. Neuroscience *71*, 55–75.

McEwen, B.S., and Morrison, J.H. (2013). The brain on stress: vulnerability and plasticity of the prefrontal cortex over the life course. Neuron *79*, 16–29.

McEwen, B.S., Nasca, C., and Gray, J.D. (2016). Stress effects on neuronal structure: hippocampus, amygdala, and prefrontal cortex. Neuropsychopharmacology *41*, 3–23.

McGarry, L.M., and Carter, A.G. (2017). Prefrontal cortex drives distinct projection neurons in the basolateral amygdala. Cell Rep. *21*, 1426–1433.

Miller, S.M., Marcotulli, D., Shen, A., and Zweifel, L.S. (2019). Divergent medial amygdala projections regulate approach-avoidance conflict behavior. Nat. Neurosci. *22*, 565–575.

Minami, C., Shimizu, T., and Mitani, A. (2017). Neural activity in the prelimbic and infralimbic cortices of freely moving rats during social interaction: effect of isolation rearing. PLoS ONE *12*, e0176740.

Mucignat-Caretta, C., Cavaggioni, A., Redaelli, M., Da Dalt, L., Zagotto, G., and Gabai, G. (2014). Age and isolation influence steroids release and chemical signaling in male mice. Steroids *83*, 10–16.

Nelson, R.J., and Trainor, B.C. (2007). Neural mechanisms of aggression. Nat. Rev. Neurosci. *8*, 536–546.

Niwa, M., Jaaro-Peled, H., Tankou, S., Seshadri, S., Hikida, T., Matsumoto, Y., Cascella, N.G., Kano, S., Ozaki, N., Nabeshima, T., and Sawa, A. (2013). Adolescent stress-induced epigenetic control of dopaminergic neurons via glucocorticoids. Science *339*, 335–339.

Papilloud, A., Veenit, V., Tzanoulinou, S., Riccio, O., Zanoletti, O., Guillot de Suduiraut, I., Grosse, J., and Sandi, C. (2019). Peripubertal stress-induced heightened aggression: modulation of the glucocorticoid receptor in the central amygdala and normalization by mifepristone treatment. Neuropsychopharmacology *44*, 674–682.

Paus, T., Keshavan, M., and Giedd, J.N. (2008). Why do many psychiatric disorders emerge during adolescence? Nat. Rev. Neurosci. *9*, 947–957.

Pellis, S.M., and Pellis, V.C. (2017). What is play fighting and what is it good for? Learn. Behav. *45*, 355–366.

Peña, C.J., Smith, M., Ramakrishnan, A., Cates, H.M., Bagot, R.C., Kronman, H.G., Patel, B., Chang, A.B., Purushothaman, I., Dudley, J., et al. (2019). Early life stress alters transcriptomic patterning across reward circuitry in male and female mice. Nat. Commun. *10*, 5098.

Pfaff, D.W. (2002). Hormones, brain and behavior (Elsevier).

Popoli, M., Yan, Z., McEwen, B.S., and Sanacora, G. (2011). The stressed synapse: the impact of stress and glucocorticoids on glutamate transmission. Nat. Rev. Neurosci. *13*, 22–37.

Qin, L., Ma, K., Wang, Z.J., Hu, Z., Matas, E., Wei, J., and Yan, Z. (2018). Social deficits in Shank3-deficient mouse models of autism are rescued by histone deacetylase (HDAC) inhibition. Nat. Neurosci. *21*, 564–575.

Raine, A., Buchsbaum, M., and LaCasse, L. (1997). Brain abnormalities in murderers indicated by positron emission tomography. Biol. Psychiatry *42*, 495–508.

Ridderinkhof, K.R., Ullsperger, M., Crone, E.A., and Nieuwenhuis, S. (2004). The role of the medial frontal cortex in cognitive control. Science *306*, 443–447.

Rosell, D.R., and Siever, L.J. (2015). The neurobiology of aggression and violence. CNS Spectr. *20*, 254–279.

Rosenkranz, J.A., and Grace, A.A. (2002). Cellular mechanisms of infralimbic and prelimbic prefrontal cortical inhibition and dopaminergic modulation of basolateral amygdala neurons in vivo. J. Neurosci. *22*, 324–337.

Roth, B.L. (2016). DREADDs for neuroscientists. Neuron *89*, 683–694.

Sayegh, J.F., Kobor, G., Lajtha, A., and Vadasz, C. (1990). Effects of social isolation and the time of day on testosterone levels in plasma of C57BL/6By and BALB/cBy mice. Steroids *55*, 79–82.

Sesack, S.R., and Carr, D.B. (2002). Selective prefrontal cortex inputs to dopamine cells: implications for schizophrenia. Physiol. Behav. *77*, 513–517.

Sharma, P.K., Wells, L., Rizzo, G., Elson, J.L., Passchier, J., Rabiner, E.A., Gunn, R.N., Dexter, D.T., and Pienaar, I.S. (2020). DREADD activation of pedunculopontine cholinergic neurons reverses motor deficits and restores striatal dopamine signaling in parkinsonian rats. Neurotherapeutics *17*, 1120–1141.

Song, Z., Kalyani, M., and Becker, J.B. (2018). Sex differences in motivated behaviors in animal models. Curr. Opin. Behav. Sci. *23*, 98–102.

Sotres-Bayon, F., and Quirk, G.J. (2010). Prefrontal control of fear: more than just extinction. Curr. Opin. Neurobiol. *20*, 231–235.

Takahashi, A., Nagayasu, K., Nishitani, N., Kaneko, S., and Koide, T. (2014). Control of intermale aggression by medial prefrontal cortex activation in the mouse. PLoS ONE *9*, e94657.

Tan, T., Wang, W., Williams, J., Ma, K., Cao, Q., and Yan, Z. (2019). Stress exposure in dopamine D4 receptor knockout mice induces schizophrenia-like behaviors via disruption of GABAergic transmission. Schizophr. Bull. *45*, 1012–1023.

Tóth, M., Halász, J., Mikics, E., Barsy, B., and Haller, J. (2008). Early social deprivation induces disturbed social communication and violent aggression in adulthood. Behav. Neurosci. *122*, 849–854.

Walker, D.M., Cunningham, A.M., Gregory, J.K., and Nestler, E.J. (2019). Long-term behavioral effects of post-weaning social isolation in males and females. Front. Behav. Neurosci. *13*, 66.

Wall, V.L., Fischer, E.K., and Bland, S.T. (2012). Isolation rearing attenuates social interaction-induced expression of immediate early gene protein products in the medial prefrontal cortex of male and female rats. Physiol. Behav. *107*, 440–450.

Wang, W., Rein, B., Zhang, F., Tan, T., Zhong, P., Qin, L., and Yan, Z. (2018). Chemogenetic activation of prefrontal cortex rescues synaptic and behavioral deficits in a mouse model of 16p11.2 deletion syndrome. J. Neurosci. *38*, 5939–5948.

Wei, J., Yuen, E.Y., Liu, W., Li, X., Zhong, P., Karatsoreos, I.N., McEwen, B.S., and Yan, Z. (2014). Estrogen protects against the detrimental effects of repeated stress on glutamatergic transmission and cognition. Mol. Psychiatry *19*, 588–598.

Wei, J., Zhong, P., Qin, L., Tan, T., and Yan, Z. (2018). Chemicogenetic restoration of the prefrontal cortex to amygdala pathway ameliorates stress-induced deficits. Cereb. Cortex *28*, 1980–1990.

Wellman, C.L., Bangasser, D.A., Bollinger, J.L., Coutellier, L., Logrip, M.L., Moench, K.M., and Urban, K.R. (2018). Sex differences in risk and resilience: stress effects on the neural substrates of emotion and motivation. J. Neurosci. *38*, 9423–9432.

Xu, H., Liu, L., Tian, Y., Wang, J., Li, J., Zheng, J., Zhao, H., He, M., Xu, T.L., Duan, S., and Xu, H. (2019). A disinhibitory microcircuit mediates conditioned social fear in the prefrontal cortex. Neuron *102*, 668–682.e5.

Yuen, E.Y., Wei, J., Liu, W., Zhong, P., Li, X., and Yan, Z. (2012). Repeated stress causes cognitive impairment by suppressing glutamate receptor expression and function in prefrontal cortex. Neuron *73*, 962–977.

Zaydman, M.A., and Cui, J. (2014). PIP2 regulation of KCNQ channels: biophysical and molecular mechanisms for lipid modulation of voltage-dependent gating. Front. Physiol. *5*, 195.

Zelikowsky, M., Hui, M., Karigo, T., Choe, A., Yang, B., Blanco, M.R., Beadle, K., Gradinaru, V., Deverman, B.E., and Anderson, D.J. (2018). The neuropeptide Tac2 controls a distributed brain state induced by chronic social isolation stress. Cell *173*, 1265–1279.e19.

Zhang, X., and Li, B. (2018). Population coding of valence in the basolateral amygdala. Nat. Commun. *9*, 5195.

Zhong, P., Vickstrom, C.R., Liu, X., Hu, Y., Yu, L., Yu, H.G., and Liu, Q.S. (2018). HCN2 channels in the ventral tegmental area regulate behavioral responses to chronic stress. eLife *7*, e32420.

Zhou, T., Zhu, H., Fan, Z., Wang, F., Chen, Y., Liang, H., Yang, Z., Zhang, L., Lin, L., Zhan, Y., et al. (2017). History of winning remodels thalamo-PFC circuit to reinforce social dominance. Science *357*, 162–168.

STAR★METHODS

KEY RESOURCES TABLE

REAGENT or RESOURCE	SOURCE	IDENTIFIER
Bacterial and virus strains		
AAV8-CaMKIIα-hM3D (Gq)-mCherry	Addgene	Cat# 50476-AAV8
AAV8-CaMKIIα-hM4D(Gi)-mCherry	Addgene	Cat# 50477-AAV8
AAV8-CaMKIIα-GFP	Addgene	Cat# 50469-AAV8
Chemicals, peptides, and recombinant proteins		
Clozapine *N*-oxide dihydrochloride	Tocris	Cat# 6329
Bicuculline	Sigma	Cat# 14340
D-APV	Tocris	Cat# 0105
CNQX	Sigma	Cat# C127
Experimental models: organisms/strains		
Mouse: C57BL/6J	The Jackson Laboratory	Cat# 000664
Software and algorithms		
ANY-maze 5.1	Stoelting	N/A
Clampfit 10.0.7	Molecular Devices	N/A
Mini Analysis 6.0.3	Synaptosoft	N/A
Plexon Offline Sorter (Version 4.5.0.1)	Plexon	N/A
NeuroExplorer (Version 5.012)	Nex Technologies	N/A
MATLAB (Version 7.14)	MathWorks	N/A
Prism 8.0.1	GraphPad	N/A

RESOURCE AVAILABILITY

Lead contact

Further information and requests for reagents and resources may be directed to, and will be fulfilled by, the Lead Contact, Dr. Zhen Yan (zhenyan@buffalo.edu).

Materials availability

This study did not generate new unique reagents.

Data and code availability

Code generated in this study are available upon request from the Lead Contact.

EXPERIMENTAL MODEL AND SUBJECT DETAILS

Animal subjects

All experiments were performed with the approval of the Institutional Animal Care and Use Committee (IACUC) of the State University of New York at Buffalo. C57BL/6J mice were maintained in the animal facility under controlled environmental conditions (22°C, 12-hour light/dark cycle) with free access to food. Both male and female mice were utilized in all studies. All experiments were performed on mice between the age of 21 days-4 months.

METHOD DETAILS

Social isolation stress

All experiments were performed with the approval of the Institutional Animal Care and Use Committee (IACUC) of the State University of New York at Buffalo. C57BL/6J mice were maintained in the animal facility under controlled environmental conditions

(22°C, 12-hour light/dark cycle) with free access to food. Both male and female mice were randomly assigned into either single-housed (SI) or group-housed (GH) after weaning (postnatal day 21) for 5 weeks (Walker et al., 2019). Sensory cues were not limited, which means they could see, hear, and smell other animals in the colony and experienced normal husbandry procedures. Experiments were carried out by investigators in a blind fashion (with no prior knowledge about the groups and treatments).

Behavioral testing

The light was adjusted to dim during all behavioral experiments. ANY-maze 5.1 (Stoelting) was used for behavioral recording and data analysis.

Resident-intruder (RI) test

A modified protocol (Márquez et al., 2013; Wei et al., 2018) was used. Briefly, the mouse was single-housed for 24 hr, then it was exposed to an intruder (a slightly smaller (5%–15% lighter) unfamiliar control mouse of the same sex) in the home cage for 10 min. Attack behaviors of the resident mouse against the intruder, including lateral threat, upright posture, clinch attack, keep down, and chase (Koolhaas et al., 2013) were scored to measure aggression level. Non-offensive social behaviors in the RI test, including social explore, anogenital sniffing, and social groom, were counted as "no attack" together with no interaction.

Social approach (SA) test

The test animal was habituated in an apparatus (L: 57 cm, W: 43 cm, H: 43 cm) containing an empty capsule for 5 min. Then a social stimulus (an unfamiliar age- and sex-matched control mouse) was placed inside the capsule (an inverted pencil cup, D: 10.2 cm, H: 10.5 cm) (Qin et al., 2018). The test animal was put back into the apparatus to explore for 10 min. Social interaction was defined as the active seeking and sniffing of the social stimulus. Interaction time was measured with ANY-maze software, which counted the time that the test animal spent at the proximity of the capsule (the distance of animal head to cup edge: $\leq$ 3.5 cm) (Qin et al., 2018). The time spent on interacting with the social stimulus and the number of bouts approaching and engaging in social interaction were measured.

To explore the behavioral outcomes of social isolation in both males and females, animals were first subjected to the SA test, followed by the RI test one day later. In the chemogenetic experiments, males only had the RI test, and females only had the SA test.

Viral vectors and injection

Adeno-associated viruses AAV8-CaMKIIα-hM3D (Gq)-mCherry (4.1 × 10^{12} vp/ml) and AAV8-CaMKIIα-hM4D(Gi)-mCherry were obtained from Addgene. Stereotaxic injection of the virus (1 μl) to the target brain region was performed as described previously (Wang et al., 2018). In brief, mice were anesthetized and placed on a stereotaxic apparatus (David Kopf Instruments). The injection was performed with a Hamilton syringe (needle gauge 31) at a speed of 0.1 μl/min, and the needle was kept in place for an additional 5 min after injection. The virus was delivered bilaterally to the target area using the following coordinates from the bregma, mPFC: +1.98 mm anteroposterior (AP), ± 0.25 mm mediolateral (ML), −2.2 mm dorsoventral (DV); BLA: −1.46 mm AP; ± 2.8 mm ML, −4.9 mm DV; VTA: −3.64 mm AP; ± 0.5 mm ML, −4.2 mm DV. Two to three weeks after surgery, animals were used for testing. Water-soluble CNO (Tocris, #6329) was used and dissolved in saline to make the stock solution (1 mg/ml) and further diluted with saline for *in vivo* or *in vitro* application. Animals were injected with CNO (3 mg/kg, i.p.) or saline control using the counterbalanced administration order. *In vitro* electrophysiological recordings were conducted 1-6 hr after i.p. injection of CNO or saline. For no-DREADD controls, AAV8-CaMKIIα-GFP (5.1 × 10^{12} vp/ml) was injected into mPFC as described previously (Wang et al., 2018).

In vivo recording

Surgical implantation of the electrode array, *in vivo* electrophysiological data acquisition and analyses were similar to what was previously described (Xu et al., 2019; Zhou et al., 2017).

Surgical implantation of the electrode array

Mice were anesthetized with Ketamine (100 mg/Kg) /Xylazine (10 mg/Kg, i.p.). After a craniotomy (1x2 mm rectangle) was made, the dura was removed. A custom-made 16-channel microelectrode array (Liu et al., 2014b) was inserted into the mPFC. The array was arranged in 4 × 4 configuration: 33 μm diameter nickel-chromium wires with formvar insulation (California Fine Wire Co.,), 0.25 mm inter-electrode spacing, impedance < 1 MΩ and gold plated using nanoZ (White Matter). Once inserted into the target brain region, the electrode was fixed to the skull with three miniature skull screws and dental cement. Mice were then placed under a heating lamp to wake up.

Electrophysiological recording of behaving mice

After 3-5 days recovery from surgery, mice were habituated for 2-3 days to the headstage (RHD2132 16-channel amplifier/accelerometer board, Part # C3335, Intan) and cable (RHD2000 6-ft Ultra-Thin SPI cable, Part # C3216, Intan) that are connected to the electrode on their heads. To ensure the animal can move freely, the cable was suspended by a helium balloon. Multichannel electrical signals were digitized at 30 KHz and recorded with Intan 512ch Recording Controller (Part #C3004, Intan) throughout the behavioral test. Animal behavior was monitored with a digital camera mounted above (100 cm) the apparatus, and recorded with ANY-maze.

Spike sorting

Spikes were separated by a band-pass filter at 250-7500 Hz. The recorded signal was an integrated signal generated by several neurons next to the microelectrode rather than a single neuron. Therefore, spike-sorting was performed to classify different neuronal firing using Plexon Offline Sorter (Plexon) and further analyzed using NeuroExplorer (Nex Technologies) or MATLAB (MathWorks). Units with low signal-to-noise (< 3.0) or a very low baseline firing rate (< 0.5 Hz) were discarded.

Unit classification and firing rate analysis

The well-isolated units were first classified into the wide-spiking putative pyramidal neuron and narrow-spiking interneuron using an unsupervised cluster algorithm based on k-means method (Xu et al., 2019).The analysis was based on the three-dimensional space defined by each neuron's half-spike width (trough to peak duration), half valley width and the mean baseline firing rate. Spikes with shorter half-spike width and half valley width were classified to be interneurons. The interneuron population was further classified into fast spike interneurons and non-fast spike interneurons based on baseline firing rate. For a given neuron, firing rates during attack/interact and no-attack/no-interact were calculated. The Change Index (CI) was used to report the activity changes during attack/social to no-attack/no-social epochs. For firing change index of aggression, CI = (Fa - Fna) / (Fa + Fna) (Fa: firing rate during attack; Fna: firing rate during no-attack). For firing change index of sociability, CI = (Fi - Fni) / (Fi + Fni) (Fi: firing rate during interaction; Fni: firing rate during no-interaction). To generate the peri-stimulus time histogram (PSTH), a 5 s window with 1 s moving step was used. A normalized Z-score (Diehl et al., 2018) was calculated (3 s before and 6 s after attack onset; 5 s before and 6 s after social interact onset; bin = 2 s, step = 0.5 s). The spike rate was first converted to Z-score = (Fi-Fm)/SDm (Fi: firing rate in the i^{th} bin; Fm: mean firing rate of overall peri-event periods (before and after event onset); SDm: standard deviation of firing rates of all peri-event periods). Z-score was then normalized to baseline (pre-event onset).

Whole-cell recording in brain slices

Whole-cell voltage-clamp recording was used to measure synaptic currents in target brain regions as previously described (Tan et al., 2019; Yuen et al., 2012). Recordings were performed on mPFC pyramidal neurons, BLA principal neurons, and VTA DA neurons.

Voltage-clamp recording of EPSC, IPSC and I_h

Mouse brain slices (300 μm) were positioned in a perfusion chamber attached to the fixed stage of an upright microscope (Olympus) and submerged in continuously flowing oxygenated (95% O_2/5% CO_2) ACSF (in mM: 130 NaCl, 26 $NaHCO_3$, 1 $CaCl_2$, 5 MgCl2, 3 KCl, 1.25 NaH_2PO_4, 10 glucose, pH 7.4, 300 mOsm). For EPSC recordings, the pipette contained the following solution (in mM: 130 Cesium-methanesulfonate, 10 CsCl, 4 NaCl, 10 HEPES, 1 $MgCl_2$, 5 EGTA, 2 QX-314, 12 phosphocreatine, 5 MgATP, 0.2 Na_3GTP, 0.1 leupeptin, pH 7.2-7.3, 265-270 mOsm). For IPSC recording, the internal solution contained (in mM: 100 CsCl, 30 N-methyl-D-glucamine, 10 HEPES, 4 NaCl, 1 $MgCl_2$, 5 EGTA, 2 QX-314, 12 phosphocreatine, 5 MgATP, 0.5 Na_2GTP, pH 7.2-7.3, 265-270 mOsm). Holding potential was set at −70 mV for EPSC (10 μM bicuculline and 25 μM D-APV added in ACSF) and IPSC (25 μM CNQX and D-APV added in ACSF) recordings. Evoked EPSC or IPSC was elicited by a series of current pulses (50-130 μA, delivered at 0.05 Hz) from S48 stimulator (Grass Technologies) via a bipolar stimulating electrode (FHC) that placed ~100 μm apart from the recording neuron. In VTA DA neurons, I_h current was recorded with a series of voltage steps from −130 mV to −70 mV (3 s, 10 mV interval) from a holding potential at −70 mV (Friedman et al., 2014) with the same internal and external solution for AP recording.

Current-clamp recording of spontaneous AP and evoked AP

To record the spontaneous (sAP) and evoked action potential (eAP), slices were bathed in a modified ACSF (in mM: 130 NaCl, 26 $NaHCO_3$, 1 $CaCl_2$, 0.5 $MgCl_2$, 3.5 KCl, 10 glucose, 1.25 NaH_2PO_4) to slightly elevate the basal neuronal activity (Maffei et al., 2004; Maffei and Turrigiano, 2008; Wang et al., 2018). Whole-cell current-clamp was used with the internal solution containing (in mM: 20 KCl, 100 K-gluconate, 10 HEPES, 4 ATP, 0.5 GTP, and 10 phosphocreatine). For sAP recording in the BLA, a small depolarizing current (< 100 pA) was applied to adjust the inter-spike membrane potential between −60 mV and −55 mV. For the sAP recording in the VTA DA neurons, no current injection was applied. For evoked action potential, membrane potential was adjusted to −70 mV while steps of depolarizing currents (−30 pA to 300 pA) were injected. Whole-cell recording data were analyzed with Clampfit 10.0.7 (Molecular Devices) and Mini Analysis 6.0.3 (Synaptosoft).

Imaging

To verify the electrode placement, a 12 μA direct current was applied in each channel for 30 s. Anathetized animals were transcardially perfused with 0.1 M phosphate buffer saline (PBS) followed by 4% paraformaldehyde (PFA, in 0.1 M PBS). Brains were removed and post-fixed in 4% PFA for 2 days, and then transferred into 30% sucrose overnight before sectioning into 100 μm slices coronally. Images were acquired using a Leica DMi8 fluorescence microscope.

QUANTIFICATION AND STATISTICAL ANALYSIS

GraphPad Prism 8.0.1 (GraphPad Software) was used for statistical analysis of the data. All data were presented as means ± SEM. Experiments with two groups were analyzed using t tests (one-tail or two-tailed, unpaired or paired), unless the data failed Shapiro-Wilk tests for normality, in which case the data were subjected to Mann-Whitney U (M-W) test or Kolmogorov-Smirnov (K-S) test. Experiments with more than two groups were subjected to one-way ANOVA, two-way ANOVA, or two-way repeated-measure ANOVA (rmANOVA), followed by post hoc tests for multiple comparisons. A chi-Square test was used in the pie chart of proportions. Detailed statistics are reported in Table S1. The use of asterisks indicate statistical significance (# $p < 0.1$, * $p < 0.05$, ** $p < 0.01$, *** $p < 0.001$).